

# Microbially influenced corrosion and rust tubercle formation on sheet piles in freshwater systems

Annika Fiskal<sup>1</sup>  | Jeremiah Shuster<sup>2,3</sup> | Stefan Fischer<sup>2,3</sup> | Prachi Joshi<sup>3</sup> | Lipi Raghunatha Reddy<sup>4</sup> | Sven-Erik Wulf<sup>5</sup>  | Andreas Kappler<sup>2,3,6</sup> | Helmut Fischer<sup>1</sup> | Ilona Herrig<sup>7</sup> | Jutta Meier<sup>8</sup>

<sup>1</sup>Department U2—Microbial Ecology, Federal Institute of Hydrology, Koblenz, Germany

<sup>2</sup>Tübingen Structural Microscopy, University of Tübingen, Tübingen, Germany

<sup>3</sup>Geomicrobiology, Department of Geosciences, University of Tübingen, Tübingen, Germany

<sup>4</sup>Department G2—Aquatic chemistry, Federal Institute of Hydrology, Koblenz, Germany

<sup>5</sup>Section B2—Steel Structures and Corrosion Protection, Federal Waterways Engineering and Research Institute, Karlsruhe, Germany

<sup>6</sup>Cluster of Excellence: EXC 2124: Controlling Microbes to Fight Infection, Tübingen, Germany

<sup>7</sup>Department G3—Ecotoxicology, Federal Institute of Hydrology, Koblenz, Germany

<sup>8</sup>Institute for Integrated Natural Sciences, University Koblenz, Koblenz, Germany

## Correspondence

Annika Fiskal, Department U2—Microbial Ecology, Federal Institute of Hydrology, Am Mainzer Tor 1, 56068, Koblenz, Germany.  
Email: [fiskal@bafg.de](mailto:fiskal@bafg.de)

Jutta Meier, Institute for Integrated Natural Sciences, University Koblenz, Universitätsstraße 1, 56070 Koblenz, Germany.  
Email: [jmeier@uni-koblenz.de](mailto:jmeier@uni-koblenz.de)

## Funding information

Deutsche Forschungsgemeinschaft, Grant/Award Numbers: EXC2124, Project ID 390838134, INST 37/1027-1 FUGG; The German Federal Ministry for Digital and Transport

## Abstract

The extent of how complex natural microbial communities contribute to metal corrosion is still not fully resolved, especially not for freshwater environments. In order to elucidate the key processes, we investigated rust tubercles forming massively on sheet piles along the river Havel (Germany) applying a complementary set of techniques. In-situ microsensor profiling revealed steep gradients of O<sub>2</sub>, redox potential and pH within the tubercle. Micro-computed tomography and scanning electron microscopy showed a multi-layered inner structure with chambers and channels and various organisms embedded in the mineral matrix. Using Mössbauer spectroscopy we identified typical corrosion products including electrically conductive iron (Fe) minerals. Determination of bacterial gene copy numbers and sequencing of 16S rRNA and 18S rRNA amplicons supported a densely populated tubercle matrix with a phylogenetically and metabolically diverse microbial community. Based on our results and previous models of physicochemical reactions, we propose here a comprehensive concept of tubercle formation highlighting the crucial reactions and microorganisms involved (such as phototrophs, fermenting bacteria, dissimilatory sulphate and Fe(III) reducers) in metal corrosion in freshwaters.

## INTRODUCTION

In aquatic environments, unalloyed steel such as sheet piles used for locks and weirs, can corrode due to Fe<sup>0</sup> oxidation, thereby reducing structural integrity which

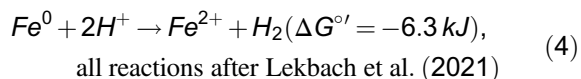
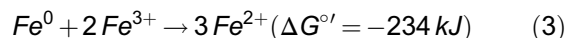
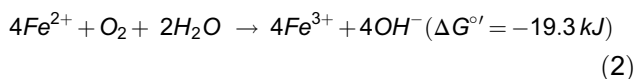
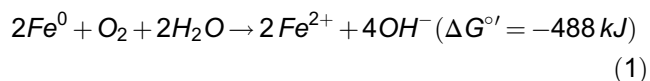
comes with safety risks (Binder & Graff, 1995; Heeling, 2017). In 2017, it was estimated that 3% to 4% of all nation's gross domestic product (GDP) constituted the prevention, maintenance or reconstruction related to damage caused by corrosion; globally, this

This is an open access article under the terms of the [Creative Commons Attribution](https://creativecommons.org/licenses/by/4.0/) License, which permits use, distribution and reproduction in any medium, provided the original work is properly cited.

© 2023 The Authors. *Environmental Microbiology* published by Applied Microbiology International and John Wiley & Sons Ltd.

corresponds to 2.5 trillion USD (Koch, 2017). Previous studies demonstrated that ~20% of corrosion can be attributed to microbially influenced corrosion (MIC) (Heitz et al., 1996; Zuo, 2007). MIC has been documented in natural environments in both seawater (Lee et al., 2004; Videla, 1994) and freshwater (Odokuma & Ugboma, 2012; Rao et al., 2000) as well as in engineered systems such as oil, gas and sewer pipelines (Crolet, 2005; Vincke et al., 2001).

Due to the occurrence of corrosion under a wide variety of environmental settings, it has been a challenge to disentangle and accurately describe the underlying (bio)chemical reactions and mechanisms. The occurrence of the different corrosion processes and the overall corrosion rate depends on various physico-chemical factors such as the presence of O<sub>2</sub> and alternative electron acceptors, conductivity, pH, redox potential, concentration of corrosive compounds and the type of corrosion products forming, which, in turn, can be all influenced by microbial activity (Heitz et al., 1996; Little et al., 2020). Under oxic conditions, the corrosion of unalloyed steels occurs primarily via the abiotic oxidation of Fe<sup>0</sup> to Fe<sup>2+</sup> involving the reduction of O<sub>2</sub> to OH<sup>-</sup> (Reaction 1). The aqueous ferrous iron is subject to further oxidation to ferric iron (Reaction 2). Although this reaction can occur abiotically, it is known to be accelerated by Fe(II)-oxidizing bacteria especially under microoxic (and/or acidic) and anoxic conditions via dissimilatory nitrate reduction (Bryce et al., 2018). Ferric iron can act as an additional oxidant forming a positive feedback loop (Reaction 3). Additionally, under anoxic conditions, abiotic corrosion occurs by the reduction of H<sup>+</sup> (Reaction 4).



While O<sub>2</sub> and NO<sub>3</sub><sup>-</sup> are relatively strong oxidants, microbial catalysis also allows the coupling of the oxidation of Fe<sup>0</sup> to Fe<sup>2+</sup> to less favourable electron acceptors such as SO<sub>4</sub><sup>2-</sup> or CO<sub>2</sub> (Li et al., 2018). The low redox potential of the redox couple Fe<sup>2+</sup>/Fe<sup>0</sup> (E<sup>o'</sup> = -447 mV) makes Fe<sup>0</sup> a favourable electron donor for anaerobic respiration. Fe<sup>0</sup> oxidation under anoxic conditions is thought to take place via three main mechanisms: (i) H<sub>2</sub>-mediated iron-to-microbe

electron transfer (HIMET), (ii) shuttle mediated iron-to-microbe electron transfer (SIMET) and (iii) direct iron-to-microbe electron transfer (DIMET) (Lekbach et al., 2021). HIMET can promote Fe<sup>0</sup> corrosion through H<sub>2</sub> consumption. Formation of H<sub>2</sub> (Reaction 4) may be even accelerated by the sequestration of extracellular hydrogenases (Enning & Garrelfs, 2014; Philips et al., 2019). SIMET uses redox-active organic molecules such as flavins, phenazines and humic acids as electron shuttles from Fe<sup>0</sup> to the bacterium (Lekbach et al., 2021; Little et al., 2020). DIMET is thought to occur via outer surface cytochromes and electrically conductive pili (Dinh et al., 2004; Holmes et al., 2019; Venzlaff et al., 2013). DIMET seems to be a common trait of highly corrosive microorganisms (Lekbach et al., 2021) as suggested for methanogens (Kip et al., 2017), sulphate-reducers (Enning et al., 2012) and nitrate-reducers (Iino et al., 2015), however, this has yet to be validated experimentally (Lekbach et al., 2021).

The sequence of reactions during the corrosion process will eventually lead to the consumption of O<sub>2</sub> and to the precipitation of corrosion products such as iron (Fe) minerals. These may block the transport of O<sub>2</sub> to the metal surface leading to microoxic and finally anoxic micro niches. This spatial separation of Fe<sup>0</sup> oxidation and O<sub>2</sub> reduction necessitates the flow of electrons from the anodic to the cathodic site through conductive substances (both organic and inorganic) and/or the availability of alternative electron acceptors at the metal surface (Sarin et al., 2004a; Sarin et al., 2004b). The presence of an electrochemical process, that is, the spatial decoupling of the anodic and the cathodic reaction, within a diffusion-limited system is indicated by a characteristic pH profile (Jin et al., 2015; Nielsen et al., 2010).

The gradient formation is reinforced by microbial colonization of the metal surface and subsequent biofilm formation. Extracellular polymeric substances (EPS) together with cell surfaces serve as nucleation sites for Fe minerals (Levett et al., 2016). The organic carbon produced by chemolithoautotrophs (and possibly phototrophs) together with the organic carbon available in the water allows chemoorganoheterotrophs to grow. High metabolic rates in combination with diffusion-limited transport mediated by the EPS matrix result in steep gradients of solutes including dissolved O<sub>2</sub> (Lee & Newman, 2003). Anoxic micrometre-scale niches enable different anaerobic microorganisms (e.g. dissimilatory nitrate, ferric iron and sulphate reducers, fermenters, methanogens and acetogens) to exist in close proximity to each other as well as to aerobes (Bond & Lovley, 2005; Kip et al., 2017; Miller et al., 2018; Philips et al., 2019). Metabolic products from anaerobic metabolisms such as nitrite, H<sub>2</sub>S and organic acids can also influence corrosion by acting as

corrosive agent and/or by removing  $\text{Fe}^{2+}$  through precipitation or further oxidation (Lewandowski & Beyenal, 2009).

The so-called ‘corrosion tubercles’ are distinctive features forming on iron metal surfaces such as unalloyed steel or cast iron in natural and engineered aqueous systems. These mound-like accumulations of corrosion products may reach sizes of several millimetres to centimetres in diameter and height, and appear to be hotspots of corrosion. Corrosion tubercles are often associated with MIC and microbial activities where shown to be a driving force of tubercle formation (Jin et al., 2015). Formation of tubercles have been reported from different environments but only few studies exist from natural freshwater sites (Odokuma, 2012; Phan et al., 2020; Price et al., 2020; Ray et al., 2010b). Several studies investigated the morphology and the mineral composition of these tubercles (Albahri et al., 2019; Ray et al., 2010b; Sarin et al., 2001). However, seldomly these investigations were combined with the molecular analysis of the microbial community in order to highlight MIC (Jin et al., 2015; Kip et al., 2017) and/or with the measurement of high resolution concentration profiles of solutes in order to confirm the occurrence of electrochemical processes (Jin et al., 2015; Lee & de Beer, 1995).

As corrosion tubercles are a widespread phenomenon on sheet piles within German waterways (Kunz et al., 2001; Kunz & Binder, 2003) we aimed for a comprehensive and detailed investigation of representative tubercles in order to determine key processes and key microorganisms that govern the corrosion of metal iron in natural freshwater systems. Our study is the first to measure micro profiles of  $\text{O}_2$ , redox potential, pH,  $\text{H}_2\text{S}$  and  $\text{H}_2$  in the tubercles directly in the field. The gradients were then related to the tubercle’s morphology (visualized by micro-computed tomography ( $\mu\text{CT}$ ) and scanning electron microscopy (SEM)), mineralogy (Mössbauer spectroscopy), the composition of microbial communities (analysed by 16S- and 18S-rRNA amplicon sequencing) and the distribution of their potential metabolic functions (according to annotation by FAPROTAX).

## MATERIALS AND METHODS

### Site description and sampling

Our sampling sites were located within the Havel river system, Germany, a moderately eutrophic lowland river system containing sheet pile walls in ship locks and bank walls. These sites were chosen because they contained corroded metal structures requiring maintenance or reconstruction. Safe access to the sites for sampling was made possible through the Waterways and Shipways Office (WSA Oder-Havel) in Eberswalde,

Germany. We sampled tubercles from two locks in the Upper-Havel Waterway (Regow, RG and Himmelpfort, HO) and from a bank wall of the Lower-Havel Waterway (Ketzin, Ke) (Figure 1). For DNA extraction, Mössbauer Spectroscopy,  $\mu\text{CT}$  and SEM, tubercles were removed from the metal structures using either a sterile metal spatula (i.e. cleaned with 70% ethanol between sampling) or a single-use sterile plastic spatula. All samples were stored in sterile containers.

In November 2020, sampling at RG was possible during a routine inspection when water was drained from the lock. In-situ microsensor profiling and tubercle sampling at RG were performed within 24 h after drainage. Hence, the tubercles, which were normally permanently submersed (approx. 1.0–1.5 m below the lowest water level), were exposed to air at the time of sampling, however, they still appeared hydrated. At HO, the lock was filled to its lowest water level (ca. 3 m). The tubercles were sampled within the zone of fluctuating water levels and therefore were normally intermittently submersed. In July 2021, we had access to permanently submersed tubercles at the lower bank walls at Ke. Water parameters determined at the time of sampling as well as the different analyses performed on the tubercles are listed in Table 1. As most of the analyses involved laborious techniques and, furthermore, as some of these were destructive, not all analyses could be performed on all samples. These samples collectively represented a larger geographic area, diverse hydrological conditions (water within the lock vs. open waters; permanently submersed vs. intermittently submersed) as well as different seasons (winter and summer). At the same time, visual inspection of sampled tubercles confirmed similar morphologies and patterns with respect to colour and texture. Samples also showed the growth of phototrophic biofilms on the surface. Furthermore, mussels and sponges occurred on top or in close vicinity of the tubercles. When the tubercles were removed from the steel surface, a black coloured film at the metal surface was observed, which could be easily removed revealing a bare metallic ‘shiny’ steel surface. In addition, acidification of the samples in the field led to the distinctive smell of  $\text{H}_2\text{S}$  indicative for Fe sulphides. Furthermore, gas (likely  $\text{CO}_2$ ) bubbles formed indicative for (Fe) carbonates.

### In-situ microsensor profiling

Measurements were performed using glass microelectrodes (500  $\mu\text{m}$  tip size) attached to a micromanipulator and a field microsensor system (Unisense, Aarhus Denmark). The whole setup was mounted on a magnetic plate which was fixed by strong magnets and was perpendicular to the vertical sheet piles. This allowed the sensors to move horizontally to measure within different depths of the tubercle (Figure S1 and Text S1).

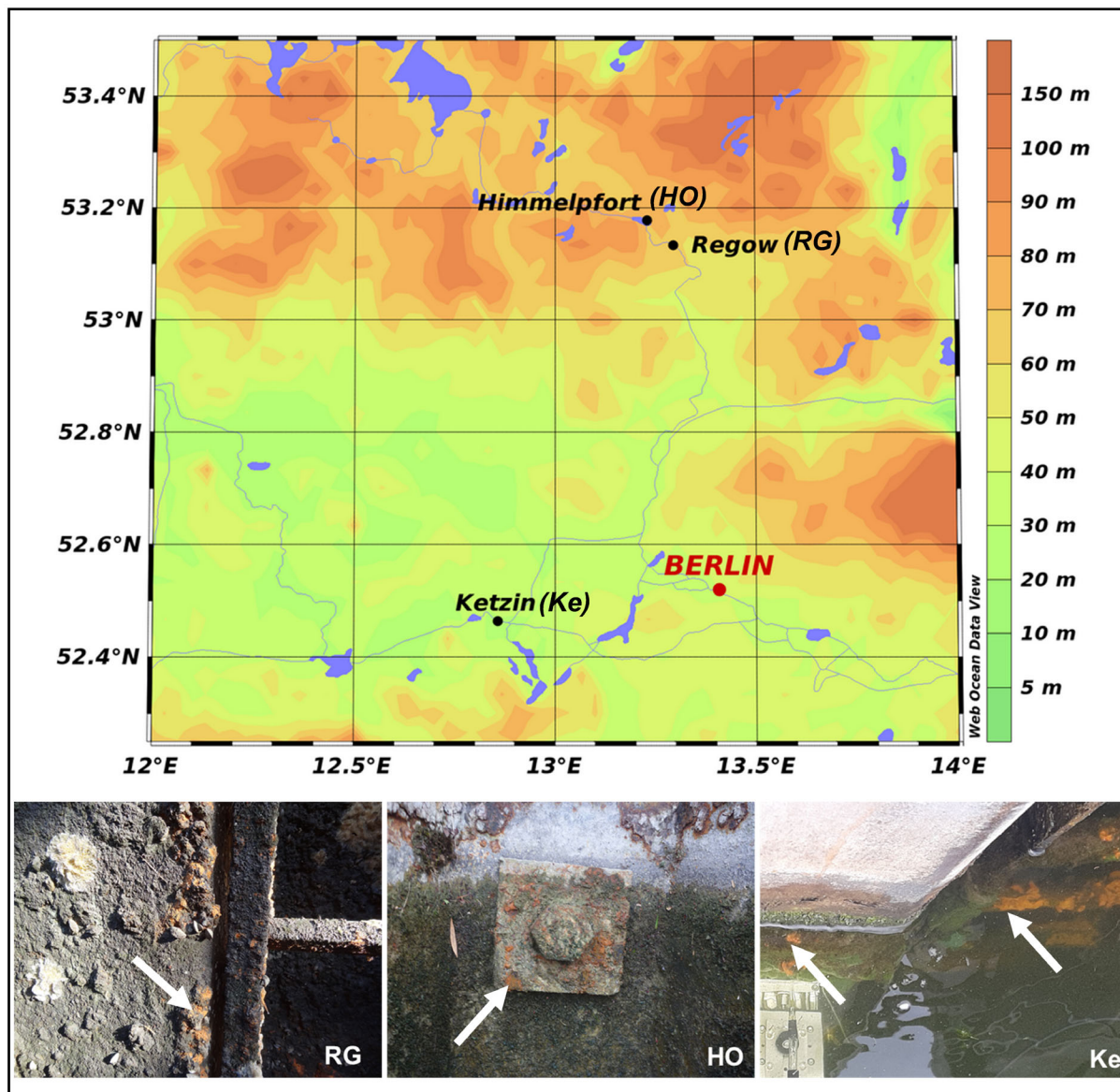


**FIGURE 1** Map of the sampling sites (HO, RG and Ke) relative to Berlin, Germany. This map was created using Ocean Data View version 5.6.2 (Schlitzer, 2022). Photographs of tubercles (arrows) growing on metals surfaces of locks or bank walls. Note that RG tubercles were only temporarily emerged (but still hydrated) at the time of sampling whereas HO and Ke tubercles were permanently submersed or within fluctuating water level.

Sensors for  $O_2$ ,  $E_h$ , pH,  $H_2$  and  $H_2S$  were used, and calibrated in the field according to the instruction manual. Briefly, the  $O_2$  sensor was calibrated with Na-L-ascorbate dissolved in 0.1 M NaOH (zero read) and with saturated river water (100% read). The  $H_2S$  sensor was calibrated using the Unisense calibration kit. The pH sensor was calibrated using pH 3.00, 4.01, 7.00 and 10.00 calibration buffers (WTW, Xylem Analytics Germany GmbH, Weilheim Germany). The  $H_2$  sensor was calibrated using a serum flask containing a gas mixture of 80%  $H_2$  and 20%  $CO_2$ . The sensor for redox potential was calibrated using a redox buffer at 124 mV. All calibration solutions were equilibrated to

the ambient air temperature (RG) or water temperature (Ke). Profiling was performed starting from the outer surface of the tubercle and penetrating into the tubercle at 500  $\mu m$  increments, at each depth triplicate measurements were performed. While in RG tubercles, sensors were not lowered all the way to the steel surface to prevent sensor damage, all sensors reached the steel surface in Ke tubercles (except for  $O_2$  sensors, where the measurement was stopped after reaching zero concentrations). Detection dwell times were 20 s per measurement and depth correction was performed by setting the tubercle surface to zero. All measurements were plotted using Grapher (Golden Software, USA).

**TABLE 1** Sampling sites, water parameters (temperature, pH, electric conductivity (EC) as well as chloride, sulphate, ammonium, nitrate and DOC concentrations) determined at the time of sampling, labelling of individual samples and corresponding analyses performed

Site	T (°C)	pH	EC ( $\mu\text{S cm}^{-1}$ )	Cl <sup>-</sup> (mg l <sup>-1</sup> )	SO <sub>4</sub> <sup>2-</sup> (mg l <sup>-1</sup> )	NH <sub>4</sub> <sup>+</sup> (mg l <sup>-1</sup> )	NO <sub>3</sub> <sup>-</sup> (mg l <sup>-1</sup> )	DOC (mg l <sup>-1</sup> )	Sample name	Microsensor	DNA	Mössbauer	$\mu\text{CT}$	SEM	
Regow	13.4	7.7	444	26	46.5	0.23	2.4	9.9	RG.P.MS1	in open air	3 sections <sup>a</sup>	3 sections <sup>b</sup>	-	-	
									RG.P.MS2	in open air	2 sections <sup>a</sup>	-	-	-	-
									RG.P.165	-	2 sections <sup>a</sup>	-	-	-	-
									RG.P.C1125	-	3 sections <sup>a</sup>	-	-	-	-
Himmel-pfort	11.1	7.4	370	18	28.8	0.07	1.7	6.6	HO.P-Anker.1	-	Bulk	Bulk	-	-	
									HO.P-Anker.2	-	Bulk	-	-	-	-
									HO.P.SW.sub	-	Bulk	-	-	-	-
Ketzin	25.4	7.9	782	82	-	0.09	2.0	-	Himmel-pfort	-	Bulk	-	whole	4 sections <sup>c</sup>	
									Ke.P.1	-	Bulk	-	-	-	-
									Ke.P.1	-	Bulk	-	-	-	-
									Ke.P.1	-	Bulk	-	-	-	-
									Ke.P.MS	under water	Bulk	-	-	-	

*Note:* Some samples were divided into different sections for various analytical techniques. Microsensor profiling was either performed in the open air (drained water lock of Regow) or under water (bank wall at Ketzin).  
<sup>a</sup>For DNA analysis material from the outer, middle (two sections) and for two samples also the inner sections (three sections) were analysed separately.  
<sup>b</sup>For Mössbauer spectroscopy, material from three sections (outer, middle and inner) were analysed separately.  
<sup>c</sup>For SEM the surface was imaged as well as three other sections (outer, middle and inner).

## Microcomputed tomography ( $\mu\text{CT}$ )

A representative HO tubercle was selected for visualization of the morphology and its biological and mineral components by  $\mu\text{CT}$  and SEM. Upon sampling, the tubercle was placed into a sterile container with river water to keep the sample completely hydrated. To fix any bacteria occurring on or within the tubercle, 25% electron microscopy-grade glutaraldehyde was added to a final concentration of 2.5%. This fixed tubercle was stored at 4°C for at least 24 h. Dehydration of the sample was started by removing the fluid (river water and glutaraldehyde mixture) and replacing it by 25%<sub>(aq)</sub> ethanol and left to incubate for 15 min. This dehydration process was continued in the same way by incubation the sample in 50%<sub>(aq)</sub>, 75%<sub>(aq)</sub> and 100% ethanol (3×). After the final ethanol dehydration step, the tubercle was submersed for 15 min into a glass flask containing a mixture of 100% ethanol and hexamethyldisilazane (HMDS). The tubercle was then transferred to a container containing ~2 ml of fresh HMDS. The lid of the container was left partially open to allow the HMDS to gradually evaporate and the samples to air dry overnight. For imaging, the tubercle was attached to an aluminium SEM sample holder by plastic conductive carbon cement (Leit-C-Plast, G3302, Plano GmbH, Wetzlar, Germany) and was sputter coated with a 10 nm thick deposition of platinum. The latter was performed as surface information of the tubercle was first imaged by SEM (see also below), before performing the  $\mu\text{CT}$  imaging.

For the  $\mu\text{CT}$  scan the sample was placed on a holder and scans were acquired using a Nikon XTH 320  $\mu\text{CT}$  scanner (Nikon Metrology, Leuven, Belgium) operated by the Visualization, Digitalization and Replication joint-lab at the Eberhard Karls University of Tübingen and Senckenberg Center for Human Evolution and Palaeoenvironment, Germany. An X-ray tube with a multi-metal reflection target with a maximum acceleration voltage of 225 kV was used and the sample was scanned with 200 kV and 35  $\mu\text{A}$ . A total of 4476 projections were acquired at 9.58532  $\mu\text{m}$  isometric voxel size, holding four frames per projection. During the scan a copper filter of 0.1 mm was used. Visualizations were created using AMIRA software (ThermoFisher Scientific, Waltham, MA).

## Scanning electron microscopy (SEM)

The tubercle, previously analysed by  $\mu\text{CT}$ , was split along preferential plains of fracture using a sterile razor blade to receive distinct cross-sections for SEM analysis. By this means, we broadly identified 'inner', 'middle', and 'outer' section from the tubercle and were subsampled. These subsamples were then attached to aluminium stubs using either conductive carbon

adhesive pads (G3347, Plano GmbH, Wetzlar, Germany) or Tempfix adhesive (G3305, Plano GmbH, Wetzlar, Germany). The samples were coated with a 10 nm thick deposition of platinum to reduce charging effects during analysis. The structure of the tubercle sections was characterized using a Zeiss Crossbeam 550 L (Carl Zeiss Microscopy GmbH, Oberkochen, Germany) focused ion beam-scanning electron microscope (FIB-SEM). Images were taken in secondary electron mode using an acceleration voltage of 2 keV.

## Mössbauer spectroscopy

Mössbauer spectroscopy was used to determine the composition of Fe minerals from one RG and one HO tubercle. The RG tubercle was split roughly into three sections (outer, middle and inner) to determine the spatial heterogeneity of the mineralogy whereas the HO tubercle was analysed as a bulk sample. All samples were prepared anoxically to preserve the redox speciation and mineralogy. Tubercles from both sites were placed into containers and immediately frozen in liquid N<sub>2</sub>. These containers were opened inside a glovebox (Mbraun Unilab Workstation, 100% N<sub>2</sub> atmosphere, <20 ppm O<sub>2</sub>) and samples were loaded into Plexiglas<sup>®</sup> holders (area 1 cm<sup>2</sup>) to form a disc. These samples were kept in airtight jars at -20°C until analysis. Sample holders were inserted into a closed-cycle exchange gas cryostat under a backflow of He to minimize exposure to air. Spectra were collected at 77 K and in some cases 5 K using a constant acceleration drive system (WissEL, Munich, Germany) in transmission mode with a <sup>57</sup>Co/Rh source. All spectra were calibrated against a 7 μm thick α-<sup>57</sup>Fe foil that was measured at room temperature. Analyses were carried out using Recoil (Lagarec & Rancourt, 1998) and the Voigt Based Fitting (VBF) routine (Rancourt & Ping, 1991). The half width at half maximum (HWHM) was constrained to 0.123 mm s<sup>-1</sup> during fitting.

## DNA extraction and quantification of bacterial copy numbers by droplet digital (dd) PCR

Tubercles for DNA extraction were immediately placed in sterile and sealable plastic containers and frozen in liquid nitrogen. Some tubercles were cleaved into outer, middle and inner sections similarly to the previous analyses. However, tubercles were still frozen when subsamples were taken therefore separation was achieved by scraping off different sections from frozen tubercles using sterile spatulas. DNA was extracted from tubercles using the Fast DNA Spin Kit for Soil and FastPrep (MP Biomedicals, Irvine, CA USA). DNA was extracted from ~0.5 g tubercle material following the

manufacturer's protocols with additional steps to optimize the yield and quality of the extracted DNA (for a detailed description see Text S2).

Absolute abundance of bacterial 16S rRNA genes were determined for all samples from which DNA was extracted by droplet digital PCR (ddPCR) using Bac908F\_mod (5'-AACTCAAAGAATTGACGGG-3')/Bac1075R (5'-CACGAGCTGACGACARCC-3') primers (biomers, Ulm, Germany). PCR reactions were performed in 22 μl total volume (10 μl QX 200 ddPCR EvaGreenSmx [Bio-Rad, Hercules, CA] 8 μl nuclease-free water, 1 μl of forward and reverse primers [250 nM], and 2 μl of DNA template). The DNA template was diluted 1:100, 1:1000, 1:10,000 and 1:100,000 for 16S rRNA analysis. 20 μl of the reaction mix were used to generate droplets (Bio-Rad QX200 Droplet Generator, Bio-Rad, Hercules, CA). The resulting emulsion (40 μl) was transferred to a 96-well plate and sealed. PCR was run in a Bio-Rad C1000-Touch Thermal Cycler. The amplification conditions were as follows: 5 min at 95°C; 40 cycles of 10 s at 95°C, 30 s at 55°C and 15 s at 72°C (ramp rate 2°C s<sup>-1</sup>). Enzymes were deactivated by a 5 min hold at 4°C, followed by a 5 min hold at 90°C. Each run included a non-template control (nuclease free water) and a positive control (digested gDNA of *Shewanella baltica* DSMZ 9439). Droplets were read on a Bio-Rad QX200 Droplet Reader. Only samples with at least 11,000 accepted droplets were used for further analysis. The positive droplet threshold was set manually using the QuantaSoft™ Analysis Pro software (Bio-Rad, Hercules, CA). Gene abundance (copies per μl) was corrected for initial dilution of DNA template and dilution of the reaction volume during droplet generation. Gene copies per gram sample (tubercle material, wet weight) were calculated.

## 16S rRNA and 18S rRNA amplicon sequencing

16S rRNA amplicon sequencing was performed on all samples whereas 18S rRNA amplicon sequencing was only performed on the samples which were separated into different sections (outer, middle, inner). Sequencing was performed by Novogene Co. (Ltd, Beijing, China). DNA extracts were sent on dry ice to Novogene (UK) Company Limited (Cambridge, UK) where their standard workflow was performed (Text S3). 16S rRNA amplicons were generated using 16S rRNA gene (V3-V4) specific primers (341F: 5'-CCTAYGGGRBGCASCAG-3' and 806R: 5'-GGACTACNNGGGTATCTAAT-3') and 18S rRNA amplicons using 18S rRNA gene (V4) specific primers (528F: 5'-GCGGTAATTCAGCTCCAA-3' and 706R: 5'-AATCCRAGAATTTACCTCT-3'). The library was sequenced on an Illumina platform (NovaSeq 6000 System, Illumina, San Diego, CA) and 250 bp paired-end reads were generated.

To further explore 16S rRNA amplicon sequencing data (only for samples which were split into different sections), FAPROTAX (Functional Annotation of Prokaryotic Taxa, version 1.2.3. [Louca et al., 2016]) was used. This data base offers an option to automatically assign microbial processes/functional groups to the taxonomic information using the current literature on cultured strains. The output table was created using the provided collapse\_table.py script on the OTU information (.biom files) through Python. The output table was shortened based on abundance of the assigned process and general classes of processes such as chemoheterotrophy, cellolysis and ureolysis were not considered. Bubble plots were created using R.

## RESULTS

### Gradients of O<sub>2</sub>, redox potential and pH within tubercles

Rust tubercles were characterized by strong geochemical gradients in pH, redox potential and O<sub>2</sub>. Overall, these gradients were similar between the RG tubercles and the Ke tubercle (Figure 2). O<sub>2</sub> concentrations decreased from 300 μM at the surface to below the detection limit (~0.3 μM) inwards, that is, towards the bottom of tubercle at the steel surface. O<sub>2</sub> did not penetrate further than 2 mm for all samples. In one RG tubercle (RG.MS.P.2, Figure 2, middle), a small peak in O<sub>2</sub> concentration was observed at the surface. According to the decrease in O<sub>2</sub> concentrations, redox potential decreased with penetration depth. While the values at the surface varied little from +80 to +100 mV, the lowest values detected in the interior ranged from -350 to -600 mV (vs. SHE). The redox potential decreased only gradually to ~0 mV in the upper part of the tubercles and then declined sharply towards more negative values. In the Ke tubercle, a distinct zone with a redox potential from -215 to -232 mV (vs. SHE) was observed (Figure 2, right). Such zones of intermediate redox potentials were also observed in RG tubercles, but these were less pronounced. At the deepest point, redox potentials seemed to stabilize again. The lowest value was measured at the very bottom of the Ke tubercle at the steel surface. The pH decreased from 8.5–9 at the surface to ~5.5 towards the inner part of the tubercle. Similar to the profiles of redox potential, zones of sharp gradients and zones of little change were observed. In RG tubercles, a two-step pH decrease and a slight pH increase near the bottom were detected. In the Ke tubercle, we found only one major pH decrease in the upper part and a relatively prominent pH increase already considerably above the steel surface. Neither H<sub>2</sub>S nor H<sub>2</sub> was detected by micro-sensors (detection limit for H<sub>2</sub> and H<sub>2</sub>S is 0.3 μM).

### Tubercle morphology

Two perpendicular cross-sectional views revealed the internal morphology of the HO tubercle using μCT (Figure 3). The maximum height was ~6 mm and the maximum diameter was ~17 mm. Based on the grey-scale intensity of the image pixels, the tubercle was composed of four distinct compartments (1–4). The inner part of the compartment contained irregularly shaped larger chambers and other, smaller cavities (Figure 3A, B, white dashed arrows). Material surrounding the cavities appeared loosely consolidated as inferred from the distribution of dark to medium grey pixels. The outer part of each compartment was brighter (light grey to white pixels) and appeared to consist of more consolidated material (Figure 3A, B, solid white arrows) which is also visible on the SEM micrographs (Figures 4 and 5).

Overall, SEM analysis revealed that the tubercle was a complex matrix composed of microorganisms, different types of organic material and minerals with morphologies similar to Fe (oxyhydr)oxides and carbonates (Figures 4 and 5 and Figures S2 and S3). Different diatoms were abundant at the surface (Figure 4A). Some diatoms were coated by an Fe (oxyhydr)oxide precipitate (Figure S2B1) or were completely embedded in the Fe mineral matrix leaving imprints of their silica frustules when removed (Figure 4A, solid arrow). Other diatom cells appeared free of mineral precipitates (Figure S2C1). Tube-like structures, 1–2 μm in diameter (Figure 4B, dashed arrow), with morphologies similar to twisted stalks as well as prokaryotic cells with different morphologies were observed (Figure 4C, solid arrows). Larger organic structures were also detected and might represent remnants of plants, fungi and/or algae (Figure 4B, open arrows, Figure S2D1).

The outer region of the tubercle also contained diatoms embedded within the Fe mineral matrix (Figure 4D). However, here the matrix appeared to be more consolidated in comparison to the surface (Figure 4D, black arrow). Tube-like structures were coated or probably completely built up by minerals, which might be Fe(oxyhydr)oxides (Figure 4E, dashed arrows) and covered by smaller prokaryotic cells (solid white arrows) (Figure 4E and S2E1 [magnification of the upper left area of Figure 4E]). A variety of channels and cavities were observed and corresponded to those seen by μCT (Figure 4F). The cavities contained noticeable minerals with morphologies similar to Fe oxyhydr-oxide minerals (Figure 4F, dashed arrows) with microbial cells attached (Figure 4F, solid arrows; Figure S2F1).

The middle region was comprised of both loosely and highly consolidated mineral matrices (Figure 5A and S3A1), in which diatoms (solid short arrows) were embedded as well as imprints which might originate

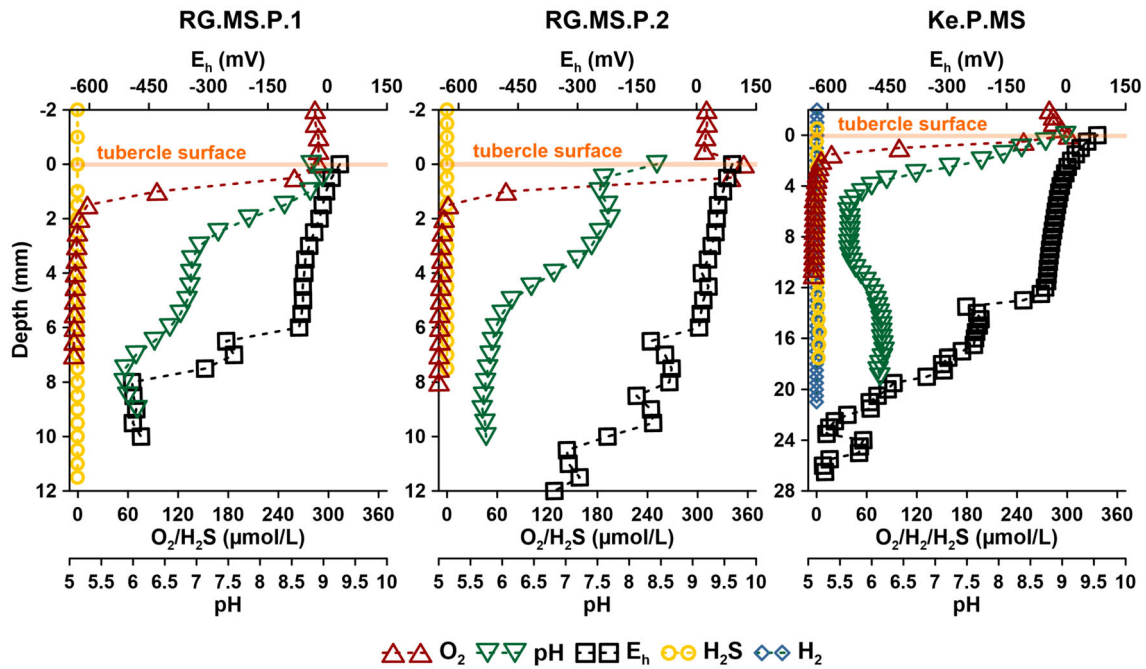


**FIGURE 2** Microsensor profiles from two tubercles at site Regow (RG) and one tubercle at site Ketzin (Ke). Note that the scaling of the y-axes differ due to the variability in tubercle thickness.

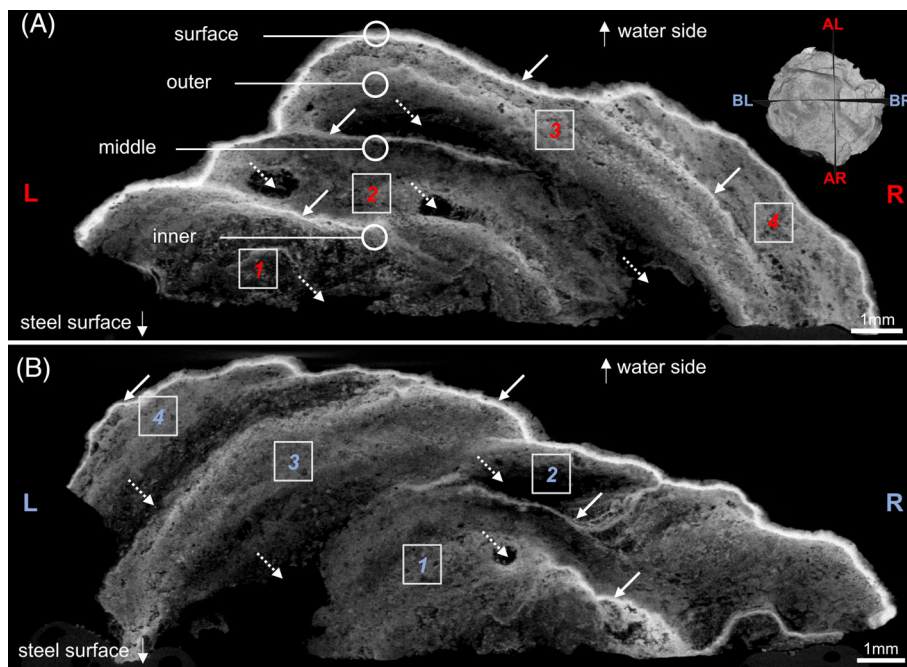


**FIGURE 3** Two perpendicular virtual cross sections (A, B, inset in A, L and R for left and right) indicate the orientation of the cross sections of the  $\mu$ CT scan of a tubercle from site Himmelpfort (HO). White circles indicate the approximate regions for SEM imaging. The  $\mu$ CT revealed distinct compartments (approximately four compartments, marked as 1–4 in boxes) with irregularly shaped cavities surrounded by more loosely consolidated material (dark to medium grey pixels, dashed arrows) and layers of more consolidated material (light grey to white pixels, solid arrows).

from cyanobacteria or algae were observed (solid long arrow). Similar to the surface and the outer region, tube-like structures were observed (Figure 5B and S3B1). Additionally, bacterial cells (solid arrows) and

probably extracellular polymeric substance (solid long arrows, Figure 5C), as well as other cells (maybe protists, Figure S3C1) were observed. Resembling the other regions, the inner region contained chamber-like

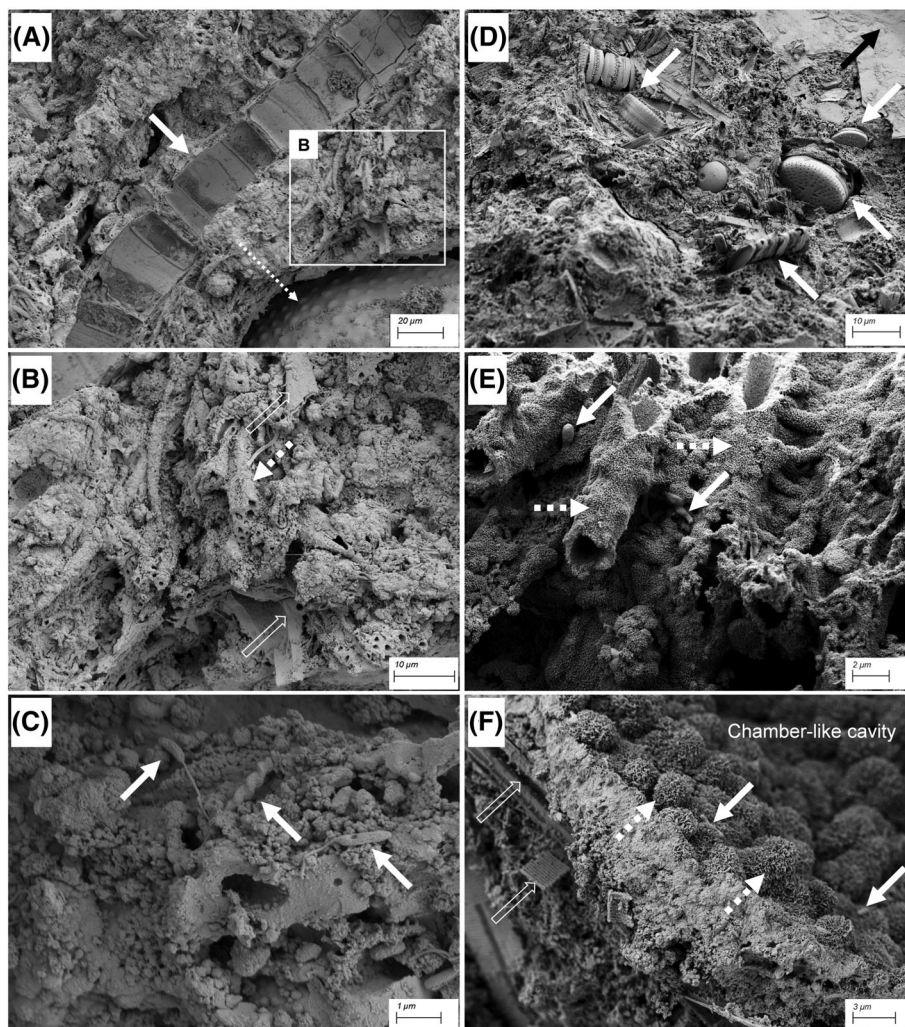


**FIGURE 4** SEM micrographs of the surface (A–C) and of the outer region of the HO tubercle (D–F). Diatoms were 10s of micrometres in size, some were partially embedded, while others appeared to leave imprints (A, white solid arrow) within the loosely consolidated matrix. Embedded bryozoans were also found (A, white dashed arrow, only a small part of the whole bryozoan can be seen, for a complete view see Figure S2, A1). Throughout the Fe mineral matrix, tube-like structures with 1–2  $\mu\text{m}$  in diameter, occurred in bundles and were often closely associated with diatoms (B, white dashed arrow, enlargement of diatom in Figure S2, B1). Plant material was also identified (white open arrows, B). At higher magnification, various flagellated rod-shaped prokaryotic cells and twisted stalks were observed among the minerals (C, white solid arrows). A variety of different diatoms (D, white solid arrows) were embedded in the consolidated Fe mineral matrix (D, black arrow). More tube-like structures (1–2  $\mu\text{m}$  in diameter) were observed. While the inner surface of these structures was smooth, the outer surface was composed of nanometre-scale acicular minerals (E, white dashed arrows). Rod-shape bacterial cells were also closely associated with the outer surface of the tube-like structures (E, white solid arrows). Chamber-like cavities were observed within this region. The interior “walls” of the cavity were consolidated and covered with “fluffy” Fe oxide minerals (F, white dashed arrows) in close association with bacterial cells (F, white solid arrows). Plant-derived material was also found (F, white open arrow).

cavities with loosely consolidated matrices (Figure 5D, F and S3D1), microorganisms embedded in more consolidated mineral matrices (Figure 5D, E black solid arrows, Figure S3E1, F1) and minerals associated to microbial cells (Figure 5F).

### Fe mineral composition based on Mössbauer spectroscopy

The Mössbauer spectra of all samples exhibited sextets at 77 K, indicating the presence of Fe oxides and/or

oxyhydroxides (Figure 6). Based on the fitting parameters, the predominant (oxyhydr)oxides were goethite ( $\alpha\text{-FeOOH}$ ) and magnetite ( $\text{Fe}_3\text{O}_4$ ) (for details regarding fitting parameters/procedures and the fitted spectra see Table S1, Text S4 and Figure S4). The three sections of the RG tubercle (RG.MS1.i, m, o) exhibited doublets indicative of green rust (GR:  $\text{Fe(III)}_x\text{Fe(II)}_y(\text{OH})_{3x+2y-z}(\text{A}^-)_z$ ;  $\text{A}^- = \text{Cl}^-$  for chloride GR, please note there is also carbonate and sulphate GR, the form of GR could not further be specified by Mössbauer spectroscopy) (Murad & Cashion, 2011; O’Loughlin et al., 2021) additionally to the (oxyhydr)oxides. The relative area of

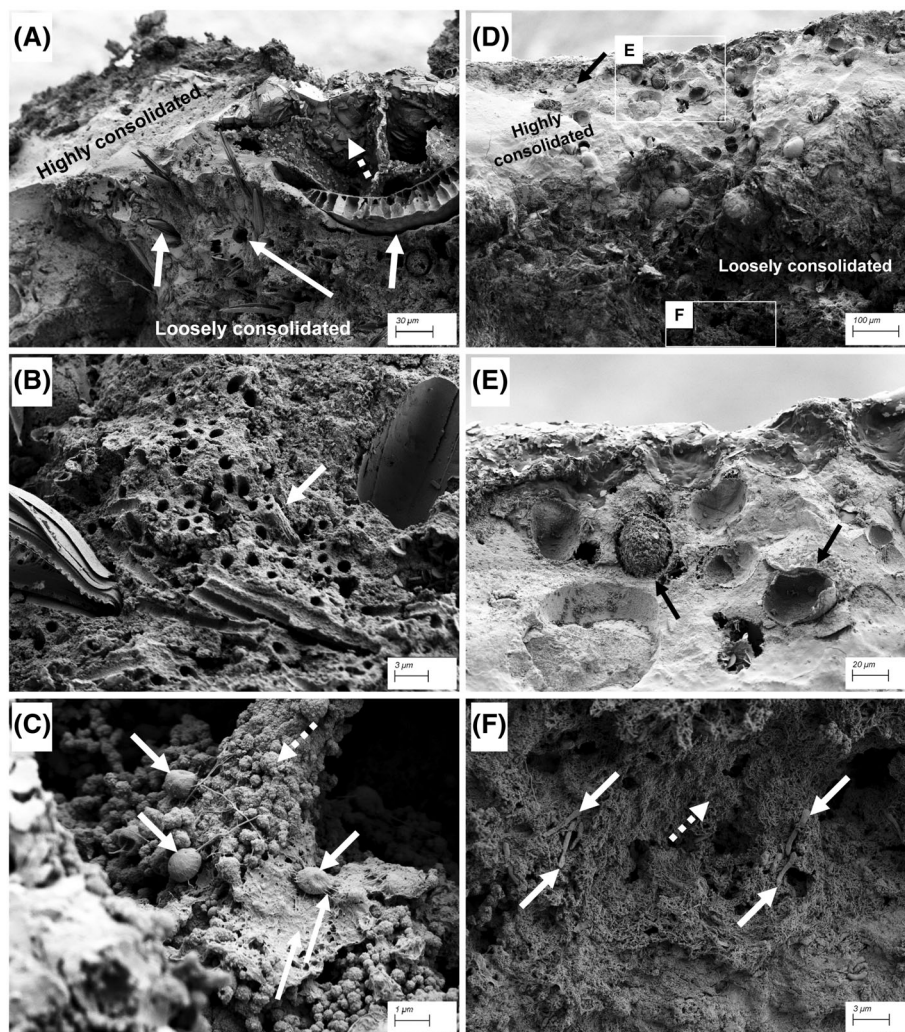


**FIGURE 5** Representative SEM micrographs of the middle (A – C) and inner (D – F) region of the HO tubercle. The consolidated mineral matrix contained euhedral minerals that were 10s of micrometres in size (A, white dashed arrow, Figure S3, A1). Loosely consolidated minerals were mostly composed of finer (nanometre-scale) minerals. Within the consolidated and loosely consolidated mineral matrix, diatoms (A, white solid arrow) and imprints of cyanobacteria or algae (A, white long arrow) were observed. Similar to the outer region, bundles of tube-like structures occurred in the mineral matrix (B, white solid arrow). Within smaller cavities, bacterial cells (C, white solid arrows), closely associated with extensive EPS (C, white long arrows), were observed on top of spherical mineral precipitates that were < 500 nm in size (C, white dashed arrow). The inner region also contained a highly consolidated mineral matrix in which presumably algae were embedded (D and E, black solid arrows). Within the loosely consolidated mineral matrix (D, F white dashed arrow), various prokaryotic cells were observed (F, white solid arrows).

goethite in those three sections ranged between 44% and 62% and decreased towards the inner parts of the tubercle, while the relative proportion of green rust increased. The percentage of magnetite appeared to stay approximately the same. Bulk analysis of the HO tubercle revealed 66% goethite, 22% magnetite and 12% lepidocrocite ( $\gamma$ -FeOOH) and no green rust was detected. Fe sulphides and Fe carbonates were not detected in any tubercle sample using Mössbauer spectroscopy.

### Bacterial abundance and microbial community composition

Bacterial copy numbers varied about two orders of magnitude from  $7.69 \times 10^7$  to  $3.64 \times 10^9$  copies  $g^{-1}$

between all samples (Figure S5). For samples that were split into different sections, higher copy numbers were found towards the outside of the tubercles.

The RG, HO and Ke tubercles contain a diverse prokaryotic and eukaryotic community (Figures S5 and S6; relative abundances in %). From the prokaryotic bacterial community, *Alpha*-, *Delta*- and *Gammaproteobacteria* were the dominant classes at all sites. Within *Deltaproteobacteria* (3%–55%, 12% on average), sulphate-reducing bacteria such as *Desulfovibrio* spp. (0.5%–49%, 5% on average), were highly abundant while *Myxococcales* (*Anaeromyxobacter*, dissimilatory Fe(III) reduction, 0.2%–7.4%, 1.2% on average) were abundant. Sulphate-reducing bacteria from the *Clostridia* (within the phylum *Firmicutes*), namely *Desulfosporosinus*, were also detected. *Rhizobiales* from the

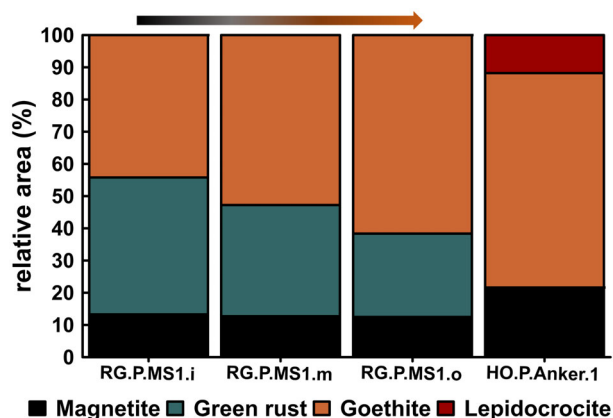


**FIGURE 6** Relative area of Fe minerals inferred from Mössbauer spectroscopy for three different sections at site Regow (RG.P.MS1.i, RG.P.MS1.m, RG.P.MS1.o) and one bulk tubercle sample at site Himmelpfort (HO.P.Anker.1). The gradient arrow indicates the layers from inner (blackish) to outer (orange-brown). The fitting parameters and spectra are given in the Figure S4 and Table S1.

*Alphaproteobacteria* class (10%–40%, 21% on average), showed high relative abundances. Within the *Gammaproteobacteria* class (8%–25%, 17% on average), nitrifying bacteria (*Nitrosomonadaceae*) and methanotrophes (*Methylococcales*) were found in high relative abundances. Other nitrifying bacteria (*Nitrospirales*) and phototrophs (*Cyanobacteria*) were also abundant in all samples. From the *Acidobacteria* class, dissimilatory Fe(III)-reducing bacteria *Geothrix* (*Holophagae*) were dominant (0.8%–27%, 4% on average). Although dominant taxa were similar between samples from all sites, some site-specific features were observed as well, for example the class *Parcubacteria* were only found in Ke tubercles.

The eukaryotic (microbial) community composition was analysed from the RG tubercles (Figure S6). At the ‘kingdom’ level within the 18S data set, three groups were distinguished (‘Metazoa’, (other) ‘Eukaryota’ and ‘Fungi’). Metazoa (Animalia) was the most dominant with 55% relative abundance, other Eukaryota was the second most dominant group with 38% relative abundance. Other Eukaryota included plants, algae, higher plants and protists (e.g. *Chlorophyta*, *Diatomea*, *Chrysophyceae*, *Streptophyta* and *Phaeophyceae*, *Apicomplexa*, *Spirotrichea*, *Oligohymenophorea*, *Litostomatea* and *Dinophyceae* as well as *Labyrinthulomycetes* (*Heterokontophyta*) and *Ichthyosporea* (*Opisthokonta*)). Fungi only occurred with 2.7% relative abundance. At the class level most samples were dominated (relative abundance) by *Phylactolaemata* (mainly *Cristatellidae*, *Christatella*) and other Bryozoa (*Gymnolaemata*, *Ctenostomatida*, *Paludicella*). The bryozoan seen in the SEM images (Figure 4A) could belong to the genus *Christatella*. Additionally, *Hydrozoa* (mainly *Limnomedusae* with *Craspedacusta*), *Ulvophyceae* (*Scotinospaera*) and *Chlorophyceae* (next to many

unidentified, mainly the genera *Desmodesmus*, *Scenedesmus* and *Mychonastes*) predominated some of the samples. Other predominant classes were *Demospongiae* (mainly *Spongillida*), *Bivalvia* (mainly *Veneroida*, *Congeria*) and *Bacillariophyceae* (*Diatomea*). Within the *Diatomea* the genera *Gyrosigma*, *Amphora*, *Staurosira* and *Navicula* were the most dominant. Some of the genera identified by sequencing can be related to the diatoms seen in the SEM images. The imprint of the diatom chain seen in Figure 4A might belong to a species of *Staurosira*. Furthermore, some species of the order *Naviculales* are probably seen in SEM Figure 4D.

## Distribution of major microbial metabolisms

The microbial community composition of RG tubercles was investigated in more detail by looking at different sections and by using sequence data to deduce the prevailing metabolisms. According to the relative abundance and the subsequent functional assignment by FAPROTAX, phototrophy, nitrification, methylotrophy, the oxidation of S compounds and Fe(II), fermentation, the dissimilatory reduction of N compounds, Fe(III) and S compounds played an important role (Figure 7). Phototrophy (oxygenic and anoxygenic) occurred in high relative abundance in all samples. As expected, the light-dependent process increased in intensity towards the outside of the tubercles. The chemolithotrophic and the methylotrophic (oxidation of C1 compounds including methane) metabolisms which often depend on O<sub>2</sub> as electron acceptor, however, did not show a consistent pattern. Whereas nitrification increased towards the outside of the tubercle, methylotrophy did not reveal such a trend. The oxidation of Fe(II) and S compounds occurred in overall low relative abundances. Fermentation was abundant in all samples, increasing towards the inside of the tubercles. The anaerobic respiration processes again did not demonstrate similar patterns along the inside-outside axis. The dissimilatory reduction of N compounds (the sum of nitrate and nitrite respiration, including denitrification and ammonification, as well as anammox) was generally less pronounced and exhibited only weak gradients. The dissimilatory reduction of Fe(III) showed no consistent trend. In contrast, the dissimilatory reduction of S compounds (including elemental sulphur, thio-sulphate, sulphite and sulphate) showed a strong gradient with increasing importance towards the inside of the tubercles and an overall higher relative share compared with the other anaerobic respiration processes.

To further explore the microbial diversity with respect to metabolic processes, taxa assigned to specific metabolisms (FAPROTAX) were looked at more closely. All taxa assigned to the processes shown in

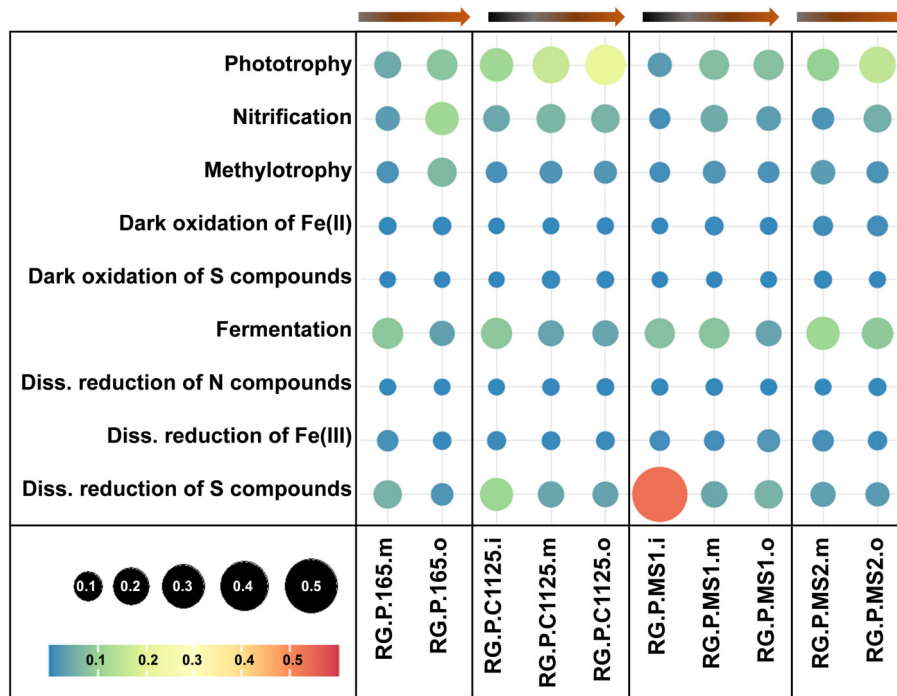


**FIGURE 7** Overview of microbial processes occurring in each sample, processes were assigned using FAPROTAX. Arrows indicate the gradient in each tubercle from black (inside) to brown (outside).

Figure 7 can be found in Table S2. The most diverse metabolisms with the highest number of taxa, namely methylotrophy, fermentation, dissimilatory reduction of N compounds, dissimilatory reduction of Fe(III) and dissimilatory reduction of S compounds are displayed in Figure 8.

Within the 16S community, *Cyanobacteria*, *Rhodospirillum rubrum* and *Rhodobacter* were assigned to contribute most to phototrophy (Table S2). Nitrification was performed by *Nitrospiraceae* and *Gallionellaceae*. The dark oxidation of S compounds was performed by *Methylobacterium*, *Thiobacillus*, *Bosea* and *Thiothrix*, whereas dark oxidation of Fe(II) was exclusively performed by *Gallionella* according to the assignment by FAPROTAX. Methylotrophy was dominated by proteobacterial groups in all samples, mainly *Methyloglobus* followed by *Methylocystis* and different taxa of the *Methylococcales*. The relative abundance of each taxa did not follow a gradient with tubercle depth. Fermentation was dominated by *Acidobacteria*, *Firmicutes* and *Proteobacteria*. Within the *Acidobacteria* only *Geothrix* was assigned to perform fermentation in the tubercles. Within the *Firmicutes*, *Clostridiales* (*Lachnospiraceae*, *Peptococcaceae*, *Desulfosporosinus*, *Peptostreptococcaceae* and *Ruminococcaceae*) were most abundant followed by *Trichococcus*. Within the *Proteobacteria*, unidentified *Gamma*proteobacteria were most abundant followed by *Aeromonas*. *Deltaproteobacteria* (*Syntrophaceae*, *Desulfobacterales*, *Desulfovibrionales*) were abundant in some samples. Even though the relative abundance of

each taxon varied in each sample, there was no consistent trend with tubercle depth. Similarly, many different taxa were assigned to perform dissimilatory reduction of N compounds. *Rhodocyclaceae* (*Dechlorosoma*, *Ferribacterium*, *Azoarcus*), were the most abundant. In some samples, *Magnetospirillum* was abundant, a weak increasing trend in relative abundance in the middle layer of the tubercle was observed. *Anaeromyxobacter*, *Arthrobacter*, *Achromobacter*, *Paracoccus* and *Bacillus* occurred in varying relative abundances without following a depth gradient. *Firmicutes* and *Proteobacteria* were assigned to perform dissimilatory reduction of Fe(III) in the samples. However, compared with dissimilatory reduction of S compounds, *Firmicutes* show higher relative abundances than *Proteobacteria*. Of the *Firmicutes*, *Desulfitobacterium* and two *Bacillus* species (*B. subterraneus*, *B. infernus*) were assigned to dissimilatory reduction of Fe(III). Representatives of the genus *Desulfitobacterium* increased in relative abundance towards the outside of the tubercle. The most abundant proteobacterial taxa was *Geobacter* followed by *Desulfovibrio desulfuricans*, *Desulfuromonas*, *Ferribacterium* and *Anaeromyxobacter*. The dissimilatory reduction of S compounds in the samples was performed by many different microbial taxa. The most abundant taxa were representatives of the genus *Desulfovibrio*. Within one tubercle, taxa from *Desulfovibrio* spp. increased in relative abundance towards the inside of the tubercle. In contrast, the family *Desulfobulbaceae* with the genera *Desulfobulbus*, *Desulfocapsa*, *Desulfurivibrio* and

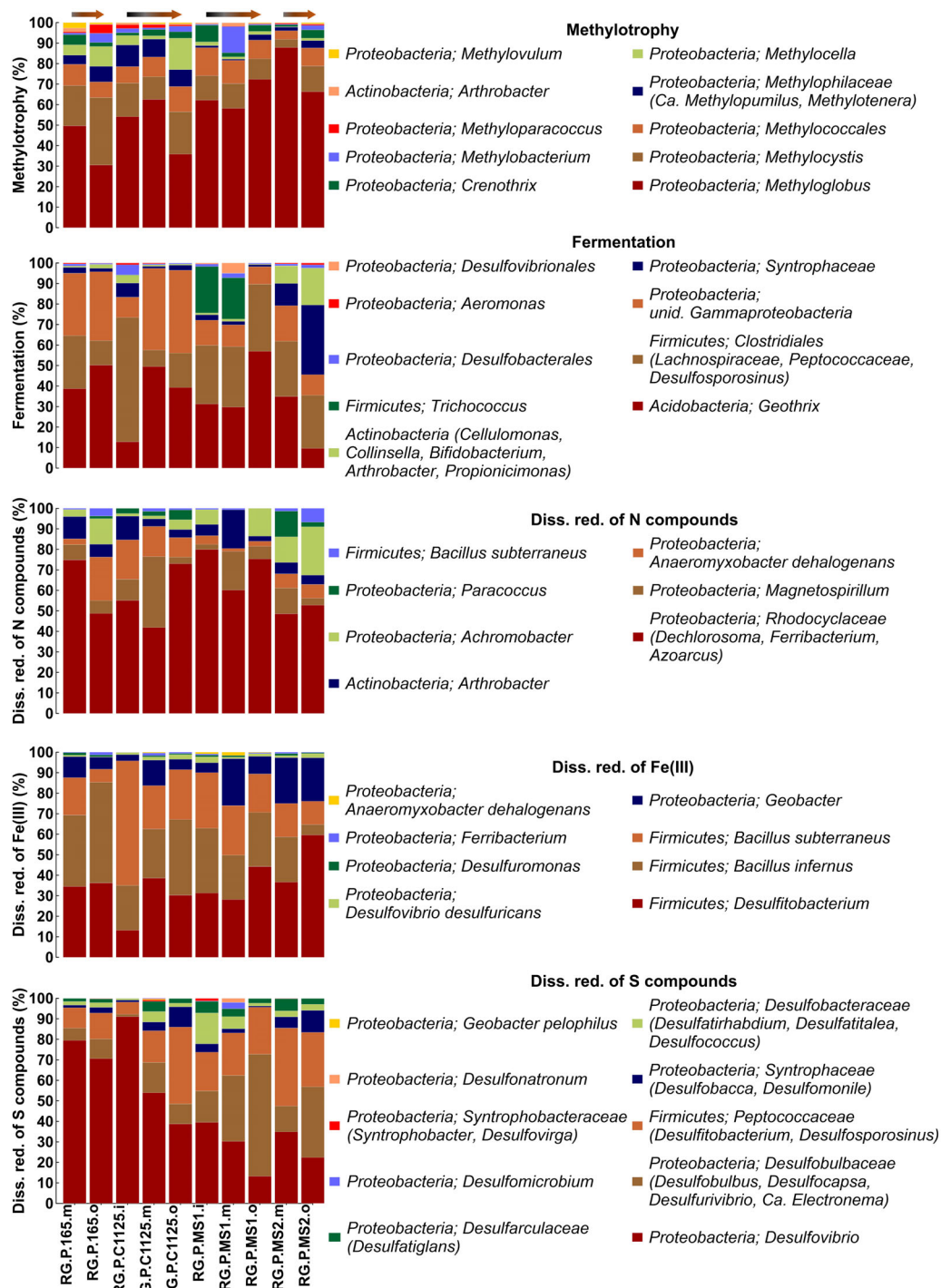


**FIGURE 8** Relative abundance of sequences assigned to the specific microbial metabolisms of methylo trophy, fermentation, dissimilatory reduction of N compounds, dissimilatory reduction of Fe(III) and dissimilatory reduction of S compounds in % based on the assignment by FAPROTAX. Bars above the plot indicate the sections of the tubercles from inside (blackish) to outside (brown-orange).

Ca. *Electronema* showed lower relative abundances towards the inner parts of the tubercles. Also abundant were the *Peptococcaceae* (*Firmicutes*) with the genera *Desulfitobacterium* and *Desulfosporosinus*, however, showing no apparent trend with tubercle depth. Methanogenesis was only assigned in a few samples and in

low relative abundance performed by *Methanomicrobia* (*Methanoregula*, *Methanosaeta*, *Methanoregula*), *Methanobacteria* and *Thermoplasmata* (*Methanomassiliococcaceae*). Nitrogen fixation was performed by *Berjerinckiacae*, *Magnetospirillum* and *Hydrogenispora* (Table S2).

## DISCUSSION

### Initial reactions of corrosion and gradient formation

The initial start of corrosion may be purely abiotic and is supposed to occur similarly in all pH-neutral freshwater environments in the presence of O<sub>2</sub> (Sarin et al., 2004b). As observed for the Havel river system, the further oxidation of Fe<sup>2+</sup> to Fe<sup>3+</sup> and the deposition of Fe(II)/Fe(III) (oxy)hydroxides lead to the formation of tubercles containing steep gradients and layered internal structures (including shell-like layers), which appear to be common features of freshwater tubercles (Jin et al., 2015; Lee & de Beer, 1995; Ray et al., 2010b; Sarin et al., 2001; Sarin et al., 2004a; Sarin et al., 2004b).

The shallow penetration and sharp decrease of O<sub>2</sub> observed in RG and Ke tubercles is indicative of high O<sub>2</sub> consumption rates near the surface, at, or in the highly consolidated layer. O<sub>2</sub> consumption may occur due to abiotic and/or microbial Fe(II) oxidation and additionally, in our case, by the oxidation of organic compounds near the surface. However, the strong pH gradient with alkaline pH values at the surface markedly above the pH in the bulk water indicated the electrochemical reduction of O<sub>2</sub> as has been also shown for marine sediments (Nielsen et al., 2010). Next to O<sub>2</sub>, also Fe(III) can be electrochemically reduced forming magnetite (Sarin et al., 2004b). Electrons may be conducted through minerals in the corrosion scale (such as magnetite) (Cornell & Schwertmann, 1996) or through Fe<sup>2+</sup> adsorbed to Fe(III) minerals such as goethite and lepidocrocite (Stratmann & Müller, 1994). All these mineral phases were detected in our tubercles. As will be discussed in more detail further below, the electrical conduction between spatially separated oxidation and reduction reactions may also be mediated by microorganisms capable of extracellular electron transfer.

In addition to the electrochemical reduction of O<sub>2</sub>, autotrophic (micro)organisms may enforce the pH increase by CO<sub>2</sub> fixation. The strong alkaline conditions at the tubercle surface did not only enhance the precipitation of Fe(II)/Fe(III) (oxyhydr)oxides but also promoted the formation of carbonates, which may contribute to the observed outer consolidated layer. Calcite has been reported from other studies to be part of the shell-like layer (Little et al., 2014; Ray et al., 2010b).

In RG tubercles, the first pH decrease closer to the tubercle surface most probably resulted from the hydrolysis of Fe(III) and precipitation of Fe(III) (oxyhydr)oxides. The zone in between was characterized by a stable pH and only a slight decrease of redox potential marking the presence of Fe(III) (oxyhydr)oxides (Kappler & Straub, 2005). The second pH decrease was indicative for Fe(II)/Fe(III) minerals such as green

rust and the formation of Fe(II) hydroxides (Jin et al., 2015). This was reflected by the opposite gradients of goethite and green rust as determined by Mössbauer spectroscopy. The more acidic zone coincided with the less consolidated interior of the tubercle. A slight increase of pH at the very bottom hinted the abiotic reduction of H<sup>+</sup>.

In the Ke tubercle, the one-step pH decrease may result from a more homogenous mineral composition as has been also shown for the HO tubercle (consisting of mainly goethite and lepidocrocite and lacking green rust). The pronounced increase of pH in the interior of the Ke tubercle strongly suggested the reduction of alternative electron acceptors and, hence, the occurrence of anaerobic respiration processes. The zone of elevated pH coincided with a stable redox potential at about –200 mV indicating dissimilatory sulphate reduction. H<sub>2</sub>S producing activities were confirmed for all tubercles by the presence of SRB and the sulfidic smell after sample acidification. Other anaerobic respiration processes were likely occurring simultaneously. The tubercle matrix provided abundant microbially reducible Fe(III) and the zones of even lower redox potentials were favourable for methanogenesis. The specific roles of the different microbial metabolic groups for tubercle formation will be outlined in the following.

### The role of phototrophy and the production of organic carbon

In the natural environment, phototrophic organisms colonize any solid surface exposed to light irrespective of the underlying material (Oberbeckmann et al., 2021). Therefore, it is not surprising to observe phototrophic biofilms covering sheet piles and corrosion scales in the Havel waterways and to find phototrophy to be a prominent prokaryotic metabolism associated with tubercles. The O<sub>2</sub> peak on the surface of the tubercle corresponded to active oxygenic photosynthetic organisms, thus phototrophy indirectly contributed to abiotic and biotic Fe(II) oxidation and hence corrosion by increasing O<sub>2</sub> concentrations (Landoulsi et al., 2011). Most importantly, phototrophs provide easily degradable organic carbon to the system by exuding low molecular weight organic compounds. Additionally, phototrophs produce polysaccharide sheaths, capsules and loose slime increasing adhesive and cohesive forces. Diatoms, which were visibly abundant in our tubercles, are known for excessive polysaccharide excretion for their gliding movement (Molino & Wetherbee, 2008). CO<sub>2</sub> fixation by phototrophs will increase the pH at the surface. Values of pH 9 are common in phototrophic biofilms or algal blooms (Kuenen et al., 1986).

As corrosion continues, the organisms are encased within the accumulating mineral precipitates, which

eventually inhibits their metabolism (Miot et al., 2015). The mineral matrix can also trap residual plant material. The incorporated polymeric organic material may be degraded within the tubercle also under anoxic conditions and may lead to the voids observed by SEM and  $\mu$ CT.

## The role of Fe(II) and S oxidizers

Though the dark oxidation of Fe(II) and S compounds appeared to be less important compared with other aerobic and anaerobic metabolisms, typical representatives were abundant and may play a decisive role in corrosion and tubercle formation. Under pH-neutral to alkaline conditions, at high O<sub>2</sub> concentrations, abiotic Fe(II) oxidation is fast (Emerson, 2018). However, at low O<sub>2</sub> concentrations within the tubercle microaerophilic Fe(II) oxidizers, such as *Leptothrix* and *Gallionella*, could thrive promoting Fe(II) oxidation and Fe(III) (oxyhydr)oxide precipitation on their extracellular polymers. *Leptothrix* spp. produce sheaths whereas *Gallionella* spp. produce twisted stalks (Suzuki et al., 2011). The encrusted tube-like structures observed in the SEM images could indeed represent sheaths of *Leptothrix* spp. Though only one OTU could be assigned to the genus *Leptothrix*, several OTUs belonged to the same family. Similarly, twisted stalks were observed by SEM and the presence of *Gallionella* spp. was further confirmed by 16S rRNA amplicon sequencing. Representatives of the genus *Gallionella* are chemolithoautotrophic, while *Leptothrix* spp. are mixotrophic or chemoorganoheterotrophic and depend on organic carbon (Emerson et al., 2010). Tube-like structures were closely associated with diatoms suggesting a possible interaction of mixotrophic Fe(II)-oxidizing bacteria and organic carbon releasing phototrophs. The occurrence of *Gallionella* and *Leptothrix* at corrosion sites and their contribution to tubercle formation have been reported for many different marine and freshwater systems (Emde et al., 1992; Emerson, 2018; Ray et al., 2010a).

Taxa assigned to perform the oxidation of S compounds (*Methylobacterium*, *Thiobacillus*, *Bosea* and *Thiothrix*) are responsible for the regeneration of sulphate which may otherwise become limiting in a freshwater environment and thereby fuelling the corrosion induced by sulphate reducers (Jørgensen, 1990). Additionally, sequences of “Ca. Electronema”, also known as ‘cable bacterium’, were identified occasionally. This organism is known to oxidize H<sub>2</sub>S in the sulfidic zone and reduce O<sub>2</sub> in the oxic zone transporting the electrons in its periplasm over a distance of several millimetres to centimetres (Kjeldsen et al., 2019). Its presence is interesting as it may contribute to the electrical conductivity within the tubercle.

## Role of anaerobic respiration and fermentation

Alternatively to O<sub>2</sub>, other terminal electron acceptors were available such as nitrate and sulphate from the Havel river water or Fe(III) produced during the corrosion process. Thus, corrosion could continue even after anoxic conditions developed within the tubercle. As alternative terminal electron acceptors were mainly provided from the water phase and their transport was diffusion-limited or consisted of solids in the outer layers, DIMET would have been the most favourable mechanism. In this case the microorganisms take advantage of the electron flow which is likely to occur within the tubercle environment connecting the anodic site with the cathodic site. HIMET and SIMET were likely to occur closely to the steel surface. Indeed, in our study, many of the identified sequences were affiliated with microorganism capable of extracellular electron transport. This and the ability to use different electron acceptors may be necessities in an environment where active movement is limited due to a densely packed mineral matrix.

Among those which were assigned to perform dissimilatory reduction of N compounds, representatives of the genus *Azoarcus* were most abundant which are also known from microbial fuel cells (Jiawei & Shaoan, 2019; Philippon et al., 2021). In addition, many representatives appeared to be involved in Fe cycling. *Dechlorosoma* is known to catalyse nitrate-reducing Fe(II) oxidation (Lack et al., 2002). *Magnetospirillum* which was abundant in some samples, is microaerophilic and can use NO<sub>3</sub><sup>-</sup> or O<sub>2</sub> as electron acceptor, furthermore it produces magnetite nanoparticles intracellularly (Schuler, 2002). Though it was assigned as nitrate-reducer, *Ferribacterium* is primarily known as Fe(III)-reducer (Cummings et al., 1999).

The most abundant proteobacterial taxa affiliated to dissimilatory Fe(III) reduction was *Geobacter*. *Geobacter* can reduce poorly soluble Fe(III) (oxyhydr)oxides by transporting the electrons via electrically conductive protein filaments (pili) (Shrestha & Rotaru, 2014) or so-called ‘nanowires’ directly to the extracellular mineral (Reguera et al., 2005). It produces high current densities in microbial fuel cells and lives in syntrophic relationships being capable of interspecies electron transfer. It has been further shown that *Geobacter* can receive its electrons directly from Fe<sup>0</sup> using it as electron donor (Tang et al., 2019). *Desulfitobacterium* can use a wide range of different electron acceptors next to Fe(III), such as sulfite. It is capable of interspecies H<sub>2</sub> transfer and uses H<sub>2</sub> concentrations below levels suitable for sulphate reduction and methanogenesis (Villemur et al., 2006). Two *Bacillus* species (*B. infernus*, *B. subterraneus*) were assigned as Fe(III)-reducers (which can also reduce Mn(IV)), *B. infernus* is strictly anaerobic but can also use NO<sub>3</sub><sup>-</sup> as electron

acceptor, whereas *B. subterraneus* is facultatively anaerobic, thus it can also use  $O_2$  (and  $NO_3^-$ ) as electron acceptor (Boone et al., 1995; Kanso et al., 2002; Xu et al., 2013). Overall, the ability to reduce Fe(III) (oxyhydr)oxides leads to the recycling of Fe(II) within the tubercle. Furthermore, some of the chambers or smaller cavities observed might be the result of this reductive dissolution process.

The dominant prokaryotes performing dissimilatory reduction of S compounds, belonged to the sulphate-reducing genus *Desulfovibrio*. Some species, like *D. ferrophilus*, are described as highly corrosive and might also perform DIMET (Liang et al., 2021). Other species use Fe(III) and/or Mn(IV) as alternative electron acceptor (*D. desulfuricans*) (Coleman et al., 1993). *Desulfovibrio* spp. were found to be predominant sulphate reducers within rust tubercles in raw reclaimed water and from a seaside harbour (Jin et al., 2015; Phan et al., 2020). The reduction of S compounds was also attributed to the taxa *Desulfobulbus* and *Desulfocapsa*. Representatives of these genera can disproportionate elemental sulphur and/or switch to fermentation when S compounds are not sufficiently available (Finster et al., 1998; Kuever et al., 2015).

Although we found low relative abundances of methanogens, their occurrence is interesting in terms of corrosion as they are considered highly corrosive and performing DIMET (An et al., 2021; Deutzmann et al., 2015; Holmes et al., 2019; Kip et al., 2017). *Methanobacterium* and *Methanosaeta* were recently found also in other corrosive biofilms. However, representatives of these genera were not reported as severely corrosive as, for example *Methanococcus maripaludis*, which harbour a special type of hydrogenases (*micH*) as well as a heterodisulphide reductase supercomplex (Hdr-SC), apparently accelerating corrosion (Lahme et al., 2021; Lienemann et al., 2018).

Fermentation appeared to be an important anaerobic metabolism with increasing relative abundance towards the inner part of the tubercle, indicating the availability of organic carbon also close to the steel surface. Fermenters provide suitable electron donors (organic acids, alcohols,  $H_2$ ) for anaerobic respiration processes. These may compete with  $Fe^0$  as electron donor possibly slowing down corrosion. However, end products of fermentation (organic acids) and end products of anaerobic respiration (nitrite, sulphide) are often corrosive themselves and can, therefore, enhance corrosion (Little et al., 2020). Interestingly, the most abundant fermenting prokaryote was *Geothrix*, which is also an Fe(III)-reducer (Coates et al., 1999). *Geothrix fermentans* is known to secrete electron shuttle compounds (Bond & Lovley, 2005). *Geothrix* has also been commonly found in other corrosion tubercles (Jin et al., 2015). *Desulfosporosinus* is also capable of sulphate and Fe(III) reduction (Pester et al., 2012). Thus, organisms able to couple fermentation to Fe(III)

reduction or even being able of dissimilatory Fe(III) reduction seem to have advantages within the tubercles.

## The formation of a multi-compartment structure

The tubercle morphology as observed in  $\mu$ CT gave valuable information about tubercle development. It was characterized by multiple compartments similar to a multi-storied building. Similar to the model proposed by Sarin et al. (2004b), corrosion products formed a scale, transport became diffusion-limited and eventually completely inhibited by a highly consolidated mineral layer. Gradients built up until eventually the chemical reactions reach equilibrium and become energetically unfavourable. However, if these highly consolidated layers broke or dissolved, due to cavity formation (degradation of incorporated organic material) or reductive dissolution of Fe(III) minerals, Fe(II)-rich tubercle pore water would extrude. It would come into contact with the oxygenated water, forming a new compartment – storey – on top of the former. The occurrence of diatom frustules and tube-like structures embedded in a mineral matrix in different sections of the tubercle suggested that the tubercle grew over time, for example the former surface was covered by new corrosion products and was now deeper inside the tubercle. This would also explain why gradients in mineral composition were partly missing or less pronounced than for pH or redox potential. In this study, redox potentials reached more negative values and pH values much lower compared with the tubercles investigated in raw reclaimed water (Jin et al., 2015). A likely explanation for this difference is that the tubercles we studied developed for a longer time and thus were older. In addition, the high microbial density and activity may have enforced the overall corrosion process.

## CONCLUSIONS

Using a multimethod approach enabled us to contribute substantially to existing models on tubercle formation (Sarin et al., 2004b) by linking physico-(electro)chemical reactions to key microbial processes as summarized in Figure 9. For one, we conclude that rust tubercles provide a favourable environment for a metabolically diverse microbial community. Its teeming prokaryotic life is not only fueled by the organic carbon synthesized by phototrophs (which is the natural source of energy for chemotrophs in a freshwater biofilm) but supplementary by the electrons released from steel. Especially microorganisms mastering extracellular electron transport may take advantage of the electrical current running through the tubercle by taking up or

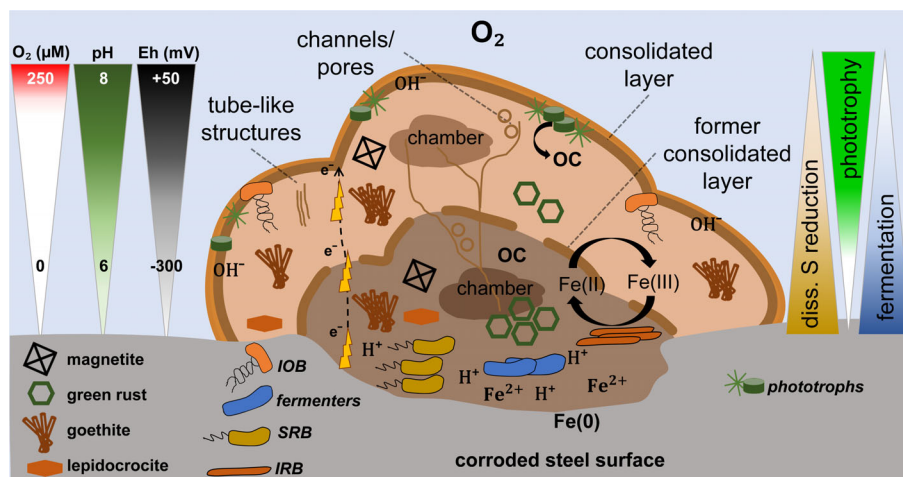


**FIGURE 9** Conceptual model of a freshwater tubercle based on previously proposed schemes by Ray et al. (2010b) and Sarin et al. (2004b). Major features are the highly complex architecture with different compartments (in the scheme only two are shown for simplicity) containing chamber-like cavities, tube-like structures and highly consolidated layers. Strong gradients of pH,  $O_2$  and redox potential occur. The relative importance of microbial metabolisms changes with penetration depth: fermentation and dissimilatory reduction of S compounds increase towards the inside, whereas phototrophy increases towards the outside of the tubercle. Labile organic carbon (OC) is provided by phototrophs supporting chemoorganoheterotrophy and mixotrophy. EPS stabilize tubercle matrix. Internal “cycling of Fe and S compounds accelerates and prolongs the overall corrosion process. A mixed mineral matrix develops over time, undergoing precipitation and re-dissolutions, some minerals are electrically conductive thus conducting electrons from anodic to cathodic sites and supporting microbes capable of extra cellular electron transport.

disposing off electrons at a suitable redox potential along the gradient. Secondly, we conclude that microbial activity is accelerating tubercle formation (e.g. by  $O_2$  and EPS production and Fe(II) oxidation) and at the same time prolonging the overall corrosion process (e.g. by dissimilatory sulphate reduction and internal S-cycling). Though tubercle formation may result from solely abiotic reactions, it would be rather slow in a natural freshwater system with low ambient temperatures, circum-neutral pH and low salt concentrations. Thirdly, we conclude that tubercle growth does not come to a stop once the highly consolidated layer is established which would impede any further exchange of solutes. Again, microbial activity is suggested to be responsible for its dissolution or breakage (e.g. by dissimilatory Fe(III) reduction and anaerobic degradation of organic matter) and, hence, for the continuation of corrosion.

## AUTHOR CONTRIBUTIONS

**Annika Fiskal:** Conceptualization (equal); data curation (equal); formal analysis (equal); investigation (equal); methodology (equal); project administration (equal); resources (equal); software (equal); validation (equal); visualization (equal); writing – original draft (lead); writing – review and editing (lead). **Jeremiah Shuster:** Conceptualization (equal); data curation (equal); formal analysis (equal); investigation (equal); methodology (equal); software (equal); validation (equal); visualization (equal); writing – original draft (equal); writing – review and editing (equal). **Stefan Fischer:** Formal analysis (equal); investigation (equal); methodology (equal);

resources (equal); software (equal); validation (equal); visualization (equal); writing – original draft (equal); writing – review and editing (equal). **Prachi Joshi:** Data curation (equal); formal analysis (equal); investigation (equal); methodology (equal); resources (equal); software (equal); validation (equal); visualization (equal); writing – original draft (equal); writing – review and editing (equal). **Lipi Raghunatha Reddy:** Investigation (equal); methodology (equal); writing – original draft (supporting); writing – review and editing (equal). **Sven-Erik Wulf:** Conceptualization (equal); data curation (equal); formal analysis (equal); investigation (equal); methodology (equal); project administration (equal); resources (equal); software (equal); validation (equal); visualization (equal); writing – original draft (equal); writing – review and editing (equal). **Andreas Kappler:** Conceptualization (equal); funding acquisition (equal); investigation (equal); methodology (equal); project administration (equal); resources (equal); supervision (equal); writing – original draft (supporting); writing – review and editing (equal). **Helmut Fischer:** Conceptualization (equal); funding acquisition (equal); resources (equal); writing – original draft (supporting); writing – review and editing (equal). **Ilona Herrig:** Conceptualization (equal); data curation (equal); formal analysis (equal); investigation (equal); methodology (equal); resources (equal); software (equal); writing – original draft (supporting); writing – review and editing (equal). **Jutta Meier:** Conceptualization (equal); formal analysis (equal); investigation (equal); methodology (equal); resources (equal); supervision (equal); validation

(equal); visualization (equal); writing – original draft (lead); writing – review and editing (lead).

## ACKNOWLEDGEMENTS

This research is part of the project RimiK (“Risk factors and indicators of MIC of hydraulic structures”) funded by the German Federal Ministry for Digital and Transport. The authors thank the Visualization, Digitalization and Replication joint-lab at the Eberhard Karls University of Tübingen and Senckenberg Centre for Human Evolution and Palaeoenvironment, Germany, for conducting the  $\mu$ CT scanning. The German Research Foundation DFG (INST 37/1027-1 FUGG) supported the acquisition of the cryogenic focused ion beam scanning electron microscope. Andreas Kappler acknowledges infrastructural support by the Deutsche Forschungsgemeinschaft (DFG, German Research Foundation) under Germany’s Excellence Strategy, cluster of Excellence EXC2124, project ID 390838134. The authors thank Bianca Konrath and Michaela Theis for technical support and data acquisition on the ddPCR. The authors furthermore thank Julia Kleinteich, Sascha Krenek and Andreas Schüttler for technical support and data discussion. Open Access funding enabled and organized by Projekt DEAL.

## CONFLICT OF INTEREST STATEMENT

The authors declare no conflict of interest.

## DATA AVAILABILITY STATEMENT

These sequence data have been submitted as BioProject under accession number PRJNA906923. <https://www.ncbi.nlm.nih.gov/sra/PRJNA906923>

## ORCID

Annika Fiskal  <https://orcid.org/0000-0001-8626-993X>  
Sven-Erik Wulf  <https://orcid.org/0000-0002-9082-2934>

## REFERENCES

- Albahri, M., Barifcani, A., Dwivedi, D., Iglauer, S., Lebedev, M., MacLeod, I.D. et al. (2019) X-ray micro-computed tomography analysis of accumulated corrosion products in deep-water shipwrecks. *Materials and Corrosion*, 70, 1977–1998. Available from: <https://doi.org/10.1002/maco.201910842>
- An, B.A., Deland, E., Sobol, O., Yao, J., Skovhus, T.L. & Koerdt, A. (2021) The differences in the corrosion product compositions of methanogen-induced microbiologically influenced corrosion (MIC) between static and dynamic growth conditions. *Corrosion Science*, 180, 109179.
- Binder, G. & Graff, M. (1995) Mikrobiell verursachte Korrosion an Stahlbauteilen. *Materials Corrosion and Materials Degradation*, 46, 639–648.
- Bond, D.R. & Lovley, D.R. (2005) Evidence for involvement of an electron shuttle in electricity generation by Geothrix fermentans. *Applied Environmental Microbiology*, 71, 2186–2189.
- Boone, D.R., Liu, Y., Zhao, Z.-J., Balkwill, D.L., Drake, G.R., Stevens, T. O. et al. (1995) *Bacillus infernus* sp. nov., an Fe(III)- and Mn(IV)-reducing anaerobe from the deep terrestrial subsurface, 45, 441–448. Available from: <https://doi.org/10.1099/00207713-45-3-441>
- Bryce, C., Blackwell, N., Schmidt, C., Otte, J., Huang, Y.M., Kleindienst, S. et al. (2018) Microbial anaerobic Fe(II) oxidation: Ecology, mechanisms and environmental implications. *Environmental Microbiology*, 20, 3462–3483. Available from: <https://doi.org/10.1111/1462-2920.14328>
- Coates, J.D., Ellis, D.J., Gaw, C.V. & Lovley, D.R. (1999) Geothrix fermentans gen. nov., sp. nov., a novel Fe(III)-reducing bacterium from a hydrocarbon-contaminated aquifer. *International Journal of Systematic Bacteriology*, 49, 1615–1622. Available from: <https://doi.org/10.1099/00207713-49-4-1615>
- Coleman, M.L., Hedrick, D.B., Lovley, D.R., White, D.C. & Pye, K. (1993) Reduction of Fe (III) in sediments by sulphate-reducing bacteria. *Nature*, 361, 436–438.
- Cornell, R. & Schwertmann, U. (1996) *The iron oxides*, 1st edition. New York: Wiley-VCH.
- Crolet, J.-L. (2005) Microbial corrosion in the oil industry: a corrosionist’s view. In: Ollivier, B., & Magot, M. (Eds.) *Petroleum Microbiology*. Washington, DC: ASM Press.
- Cummings, D.E., Caccavo, F., Jr., Spring, S. & Rosenzweig, R.F. (1999) Ferribacterium limneticum, gen. nov., sp. nov., an Fe (III)-reducing microorganism isolated from mining-impacted freshwater lake sediments. *Archives of Microbiology*, 171, 183–188.
- Deutzmann, J.S., Sahin, M. & Spormann, A.M. (2015) Extracellular enzymes facilitate electron uptake in biocorrosion and bioelectrosynthesis. *mBio*, 6, e00496-15. Available from: <https://doi.org/10.1128/mBio.00496-15>
- Dinh, H.T., Kuever, J., Mußmann, M., Hassel, A.W., Stratmann, M. & Widdel, F. (2004) Iron corrosion by novel anaerobic microorganisms. *Nature*, 427, 829–832.
- Emde, K., Smith, D. & Facey, R. (1992) Initial investigation of microbially influenced corrosion (MIC) in a low temperature water distribution system. *Water Research*, 26, 169–175.
- Emerson, D. (2018) The role of iron-oxidizing bacteria in biocorrosion: a review. *Biofouling*, 34, 989–1000. Available from: <https://doi.org/10.1080/08927014.2018.1526281>
- Emerson, D., Fleming, E.J. & McBeth, J.M. (2010) Iron-oxidizing bacteria: An environmental and genomic perspective. *Annual Review of Microbiology*, 64, 561–583. Available from: <https://doi.org/10.1146/annurev.micro.112408.134208>
- Enning, D. & Garrelfs, J. (2014) Corrosion of iron by sulfate-reducing bacteria: new views of an old problem. *Applied and Environmental Microbiology*, 80, 1226–1236. Available from: <https://doi.org/10.1128/AEM.02848-13>
- Enning, D., Venzlaff, H., Garrelfs, J., Dinh, H.T., Meyer, V., Mayrhofer, K. et al. (2012) Marine sulfate-reducing bacteria cause serious corrosion of iron under electroconductive biogenic mineral crust. *Environmental Microbiology*, 14, 1772–1787. Available from: <https://doi.org/10.1111/j.1462-2920.2012.02778.x>
- Finster, K., Liesack, W. & Thamdrup, B. (1998) Elemental sulfur and thiosulfate disproportionation by *Desulfocapsa sulfoexigens* sp. nov., a new anaerobic bacterium isolated from marine surface sediment. *Applied Environmental Microbiology*, 64, 119–125.
- Heeling, A. (2017) Ermittlung und Bewertung des Korrosionszustandes von Stahlspundwänden in Häfen und an Wasserstraßen. Kompetenz für die Wasserstraßen: Heute und in Zukunft. *Forschungs- und Entwicklungsprojekte der BAW*, 100, 39–53.
- Heitz, E., Flemming, H.C. & Sand, W. (1996) *Microbially influenced corrosion of materials: scientific and engineering aspects*, 1st edition. Berlin, Heidelberg: Springer, pp. 105–120.
- Holmes, D.E., Ueki, T., Tang, H.-Y., Zhou, J., Smith, J.A., Chaput, G. et al. (2019) A membrane-bound cytochrome enables *Methanosarcina acetivorans* to conserve energy from extracellular electron transfer. *MBio*, 10, e00789.
- Iino, T., Ito, K., Wakai, S., Tsurumaru, H., Ohkuma, M. & Harayama, S. (2015) Iron corrosion induced by nonhydrogenotrophic nitrate-reducing *Prolixibacter* sp. strain MIC1-1. *Applied and Environmental Microbiology*, 81, 1839–1846. Available from: <https://doi.org/10.1128/AEM.03741-14>

- Jiawei, Y. & Shaoan, C. (2019) Effects of using anode biofilm and cathode biofilm bacteria as inoculum on the start-up, electricity generation, and microbial community of air-cathode single-chamber microbial fuel cells. *Polish Journal of Environmental Studies*, 28, 693–700.
- Jin, J., Wu, G. & Guan, Y. (2015) Effect of bacterial communities on the formation of cast iron corrosion tubercles in reclaimed water. *Water Research*, 71, 207–218. Available from: <https://doi.org/10.1016/j.watres.2014.12.056>
- Jørgensen, B.B. (1990) The sulfur cycle of freshwater sediments: role of thiosulfate. *Limnology and Oceanography*, 35, 1329–1342.
- Kanso, S., Greene, A.C. & Patel, B.K.C. (2002) *Bacillus subterraneus* sp. nov., an iron- and manganese-reducing bacterium from a deep subsurface Australian thermal aquifer. *International Journal of Systematic Evolutionary Microbiology*, 52, 869–874. Available from: <https://doi.org/10.1099/00207713-52-3-869>
- Kappler, A. & Straub, K.L. (2005) Geomicrobiological cycling of iron. *Reviews in Mineralogy and Geochemistry*, 59, 85–108.
- Kip, N., Jansen, S., Leite, M.F.A., de Hollander, M., Afanasyev, M., Kuramae, E.E. et al. (2017) Methanogens predominate in natural corrosion protective layers on metal sheet piles. *Scientific Reports*, 7, 11899. Available from: <https://doi.org/10.1038/s41598-017-11244-7>
- Kjeldsen, K.U., Schreiber, L., Thorup, C.A., Boesen, T., Bjerg, J.T., Yang, T. et al. (2019) On the evolution and physiology of cable bacteria. *Proceedings of the National Academy of Sciences*, 116, 19116–19125.
- Koch, G. (2017) Cost of corrosion. In: *Trends in oil gas corrosion research and technologies*, Vol. 3-30. Cambridge, UK: Woodhead Publishing.
- Kuenen, J., Jørgensen, B. & Revsbech, N. (1986) Oxygen microprofiles of trickling filter biofilms. *Water Research*, 20, 1589–1598.
- Kuever, J., Rainey, F.A. & Widdel, F. (2015) *Bergey's Manual of Systematics of Archaea and Bacteria*, Vol. 1-6. New York: Springer.
- Kunz, C. & Binder, G. (2003) BAW-Brief Nr. 1-März, 2003.
- Kunz, C., Ehmann, R., Binder, G. & Meinhold, W. (2001) BAW-brief nr. 1-November, 2001.
- Lack, J., Chaudhuri, S.K., Chakraborty, R., Achenbach, L. & Coates, J.D. (2002) Anaerobic biooxidation of Fe (II) by *Dechlorosoma suillum*. *Microbial Ecology*, 43, 424–431.
- Lagarec, K., and Rancourt, D., 1998: *Mössbauer spectral analysis software for windows 1.0*. Ottawa, ON: University of Ottawa.
- Lahme, S., Mand, J., Longwell, J., Smith, R. & Enning, D. (2021) Severe corrosion of carbon steel in oil field produced water can be linked to methanogenic archaea containing a special type of [NiFe] hydrogenase. *Applied Environmental Microbiology*, 87, e01819–e01820.
- Landoulsi, J., Cooksey, K.E. & Dupres, V. (2011) Review: Interactions between diatoms and stainless steel: focus on biofouling and biocorrosion. *Biofouling*, 27, 1109–1124. Available from: <https://doi.org/10.1080/08927014.2011.629043>
- Lee, A. & Newman, D. (2003) Microbial iron respiration: impacts on corrosion processes. *Applied Microbiology and Biotechnology*, 62, 134–139.
- Lee, J., Ray, R., Lemieux, E., Falster, A. & Little, B. (2004) An evaluation of carbon steel corrosion under stagnant seawater conditions. *Biofouling*, 20, 237–247.
- Lee, W. & de Beer, D. (1995) Oxygen and pH microprofiles above corroding mild steel covered with a biofilm. *Biofouling*, 8, 273–280.
- Lekbach, Y., Liu, T., Li, Y., Moradi, M., Dou, W., Xu, D. et al. (2021) Microbial corrosion of metals-the corrosion microbiome. In: Poole, R.K. & Kelly, D.J. (Eds.) *Advances in Microbial Physiology*. London, UK: Elsevier.
- Levett, A., Gagen, E., Shuster, J., Rintoul, L., Tobin, M., Vongsvivut, J. et al. (2016) Evidence of biogeochemical processes in iron duricrust formation. *Journal of South American Earth Sciences*, 71, 131–142. Available from: <https://doi.org/10.1016/j.jsames.2016.06.016>
- Lewandowski, Z. & Beyenal, H. (2009) Mechanisms of microbially influenced corrosion. In: *Marine and industrial biofouling*. Berlin, Heidelberg: Springer-Verlag, pp. 35–64.
- Li, Y., Xu, D., Chen, C., Li, X., Jia, R., Zhang, D. et al. (2018) Anaerobic microbially influenced corrosion mechanisms interpreted using bioenergetics and bioelectrochemistry: a review. *Journal of Materials Science Technology*, 34, 1713–1718.
- Liang, D., Liu, X., Woodard, T.L., Holmes, D.E., Smith, J.A., Nevin, K. P. et al. (2021) Extracellular electron exchange capabilities of *Desulfovibrio ferrophilus* and *Desulfopila corrodens*. *Environmental Science & Technology*, 55, 16195–16203.
- Lienemann, M., Deutzmann, J.S., Milton, R.D., Sahin, M. & Spormann, A.M.J.B.T. (2018) Mediator-free enzymatic electro-synthesis of formate by the *Methanococcus maripaludis* heterodisulfide reductase supercomplex. *Bioresour Technol*, 254, 278–283.
- Little, B.J., Blackwood, D.J., Hinks, J., Lauro, F.M., Marsili, E., Okamoto, A. et al. (2020) Microbially influenced corrosion: any progress? *Corrosion Science*, 170, 108641. Available from: <https://doi.org/10.1016/j.corsci.2020.108641>
- Little, B.J., Gerke, T.L. & Lee, J.S. (2014) Mini-review: the morphology, mineralogy and microbiology of accumulated iron corrosion products. *Biofouling*, 30, 941–948.
- Louca, S., Parfrey, L.W. & Doebeli, M. (2016) Decoupling function and taxonomy in the global ocean microbiome. *Science*, 353, 1272–1277. Available from: <https://doi.org/10.1126/science.aaf4507>
- Miller, R.B., Lawson, K., Sadek, A., Monty, C.N. & Senko, J.M. (2018) Uniform and pitting corrosion of carbon steel by *Shewanella oneidensis* MR-1 under nitrate-reducing conditions. *Applied and Environmental Microbiology*, 84, e00790-18. Available from: <https://doi.org/10.1128/AEM.00790-18>
- Miot, J., Remusat, L., Duprat, E., Gonzalez, A., Pont, S. & Poinso, M. (2015) Fe biomineralization mirrors individual metabolic activity in a nitrate-dependent Fe (II)-oxidizer. *Frontiers in Microbiology*, 6, 879.
- Molino, P.J. & Wetherbee, R. (2008) The biology of biofouling diatoms and their role in the development of microbial slimes. *Biofouling*, 24, 365–379.
- Murad, E. & Cashion, J. (2011) *Mössbauer spectroscopy of environmental materials and their industrial utilization*. New York: Springer Science & Business Media.
- Nielsen, L.P., Risgaard-Petersen, N., Fossing, H., Christensen, P. B. & Sayama, M. (2010) Electric currents couple spatially separated biogeochemical processes in marine sediment. *Nature*, 463, 1071–1074.
- Oberbeckmann, S., Bartosik, D., Huang, S., Werner, J., Hirschfeld, C., Wibberg, D. et al. (2021) Genomic and proteomic profiles of biofilms on microplastics are decoupled from artificial surface properties. *Environmental Microbiology*, 23, 3099–3115.
- Odokuma, L. & Ugboma, C. (2012) Microbial corrosion of steel coupons in a freshwater habitat in The Niger Delta. *Journal of Ecology and the Natural Environment*, 4, 42–50.
- O'Loughlin, E.J., Boyanov, M.I., Gorski, C.A., Scherer, M.M. & Kemner, K.M. (2021) Effects of Fe(III) oxide mineralogy and phosphate on Fe(II) secondary mineral formation during microbial iron reduction. *Minerals*, 11, 149. Available from: <https://doi.org/10.3390/min11020149>
- Pester, M., Brambilla, E., Alazard, D., Rattei, T., Weinmaier, T., Han, J. et al. (2012) Complete genome sequences of *Desulfosporosinus orientis* DSM765(T), *Desulfosporosinus youngiae* DSM17734(T), *Desulfosporosinus meridiei* DSM13257(T), and *Desulfosporosinus acidiphilus* DSM22704(T). *Journal of Bacteriology*, 194, 6300–6301. Available from: <https://doi.org/10.1128/Jb.01392-12>
- Phan, H.C., Wade, S.A. & Blackall, L.L. (2020) Microbial communities of orange tubercles in accelerated low-water corrosion. *Applied Environmental Microbiology*, 86, e00610–e00620.

- Philippon, T., Tian, J., Bureau, C., Chaumont, C., Midoux, C., Tournebise, J. et al. (2021) Denitrifying bio-cathodes developed from constructed wetland sediments exhibit electroactive nitrate reducing biofilms dominated by the genera *Azoarcus* and *Pontibacter*. *Bioelectrochemistry*, 140, 107819.
- Philips, J., Monballyu, E., Georg, S., De Paepe, K., PrevotEAU, A., Rabaey, K. et al. (2019) An *Acetobacterium* strain isolated with metallic iron as electron donor enhances iron corrosion by a similar mechanism as *Sporomusa sphaeroides*. *FEMS Microbiology Ecology*, 95, 1–13. Available from: <https://doi.org/10.1093/femsec/fiy222>
- Price, K.A., Garrison, C.E., Richards, N. & Field, E.K. (2020) A shallow water ferrous-hulled shipwreck reveals a distinct microbial community. *Frontiers in Microbiology*, 11, 1897. Available from: <https://doi.org/10.3389/fmicb.2020.01897>
- Rancourt, D. & Ping, J. (1991) Voigt-based methods for arbitrary-shape static hyperfine parameter distributions in Mössbauer spectroscopy. *Nuclear Instruments and Methods in Physics Research Section B: Beam Interactions with Materials and Atoms*, 58, 85–97.
- Rao, T., Sairam, T., Viswanathan, B. & Nair, K. (2000) Carbon steel corrosion by iron oxidising and sulphate reducing bacteria in a freshwater cooling system. *Corrosion Science*, 42, 1417–1431.
- Ray, R.I., Lee, J.S. & Little, B.J. (2010a) Iron-oxidizing bacteria: a review of corrosion mechanisms in freshwater and marine environments. In: *Proceedings of the NACE—International Corrosion Conference Series*. San Antonio, TX, USA, pp. 14–18 March 2010.
- Ray, R.I., Lee, J.S., Little, B.J. & Gerke, T.L. (2010b) The anatomy of tubercles: a corrosion study in a fresh water estuary. *Materials and Corrosion*, 61, 993–999. Available from: <https://doi.org/10.1002/maco.201005739>
- Reguera, G., McCarthy, K.D., Mehta, T., Nicoll, J.S., Tuominen, M. T. & Lovley, D.R. (2005) Extracellular electron transfer via microbial nanowires. *Nature*, 435, 1098–1101.
- Sarin, P., Snoeyink, V., Bebee, J., Jim, K., Beckett, M., Kriven, W. et al. (2004a) Iron release from corroded iron pipes in drinking water distribution systems: effect of dissolved oxygen. *Water Research*, 38, 1259–1269.
- Sarin, P., Snoeyink, V., Bebee, J., Kriven, W. & Clement, J. (2001) Physico-chemical characteristics of corrosion scales in old iron pipes. *Water Research*, 35, 2961–2969.
- Sarin, P., Snoeyink, V., Lytle, D. & Kriven, W. (2004b) Iron corrosion scales: model for scale growth, iron release, and colored water formation. *Journal of Environmental Engineering*, 130, 364–373.
- Schlitzer, R. (2022) *Ocean data view*. Bremerhaven, Germany: Alfred Wegener Institute.
- Schuler, D. (2002) The biomineralization of magnetosomes in *Magnetospirillum gryphiswaldense*. *International Microbiology*, 5, 209–214. Available from: <https://doi.org/10.1007/s10123-002-0086-8>
- Shrestha, P.M. & Rotaru, A.-E. (2014) Plugging in or going wireless: strategies for interspecies electron transfer. *Frontiers in Microbiology*, 5, 237.
- Stratmann, M. & Müller, J. (1994) The mechanism of the oxygen reduction on rust-covered metal substrates. *Corrosion Science*, 36, 327–359.
- Suzuki, T., Hashimoto, H., Matsumoto, N., Furutani, M., Kunoh, H. & Takada, J. (2011) Nanometer-scale visualization and structural analysis of the inorganic/organic hybrid structure of *Gallionella ferruginea* twisted stalks. *Applied Environmental Microbiology*, 77, 2877–2881.
- Tang, H.-Y., Holmes, D.E., Ueki, T., Palacios, P.A. & Lovley, D.R. (2019) Iron corrosion via direct metal-microbe electron transfer. *MBio*, 10, e00303–e00319.
- Venzlaff, H., Enning, D., Srinivasan, J., Mayrhofer, K.J.J., Hassel, A. W., Widdel, F. et al. (2013) Accelerated cathodic reaction in microbial corrosion of iron due to direct electron uptake by sulfate-reducing bacteria. *Corrosion Science*, 66, 88–96. Available from: <https://doi.org/10.1016/j.corsci.2012.09.006>
- Videla, H. (1994) Biofilms and corrosion interactions on stainless steel in seawater. *International Biodeterioration & Biodegradation*, 34, 245–257.
- Villemur, R., Lanthier, M., Beaudet, R. & Lépine, F. (2006) The desulfotribacterium genus. *FEMS Microbiology Reviews*, 30, 706–733.
- Vincke, E., Boon, N. & Verstraete, W. (2001) Analysis of the microbial communities on corroded concrete sewer pipes: a case study. *Applied Microbiology and Biotechnology*, 57, 776–785.
- Xu, D., Li, Y., Song, F. & Gu, T. (2013) Laboratory investigation of microbiologically influenced corrosion of C1018 carbon steel by nitrate reducing bacterium *Bacillus licheniformis*. *Corrosion Science*, 77, 385–390.
- Zuo, R. (2007) Biofilms: strategies for metal corrosion inhibition employing microorganisms. *Applied Microbiology and Biotechnology*, 76, 1245–1253.

## SUPPORTING INFORMATION

Additional supporting information can be found online in the Supporting Information section at the end of this article.

**How to cite this article:** Fiskal, A., Shuster, J., Fischer, S., Joshi, P., Raghunatha Reddy, L., Wulf, S.-E. et al. (2023) Microbially influenced corrosion and rust tubercle formation on sheet piles in freshwater systems. *Environmental Microbiology*, 25(10), 1796–1815. Available from: <https://doi.org/10.1111/1462-2920.16393>